Chapter 4

Development of sustainable methodologies for generation of in situ Pd NPs and investigation of catalytic activity in C_{sp2}-C_{sp2} and C_{sp2}-C_{sp} bond forming reaction

This chapter is composed of two sections, illustrates the *in situ* generation of Pd NPs using non-toxic naturally abundant resources and application in Suzuki-Miyaura and Sonogashira cross-coupling reaction.

Section 4.1

Gallic acid assisted in situ generation of Pd NPs and its catalytic

application in Sonogashira cross-coupling reaction

Abstract: In this section we present a non-toxic naturally abundant phytochemical, gallic acid for *in situ* generation of Pd NPs. The method provides an efficient alternative route for Sonogashira coupling reaction under mild reaction conditions. The catalytic system displayed excellent reactivity for diverse range of substrates including less reactive aryl bromides.

4.1.1. Introduction

The C-C triple bond of alkynes is one of the most ideal functional group for the synthesis of versatile organic molecules [1,2]. The Pd/Cu-catalyzed Sonogashira coupling of aryl halides with terminal acetylene is one of the most powerful methodologies for synthesis of functionalized alkyne derivatives [3,4]. Literature reports reveal the utilization of various copper co-catalyzed palladium based system for this cross-coupling reaction [5]. However, the major drawback associated with Sonogashira reaction is the formation of side-products due to homocoupling of terminal alkynes in the presence of copper salts or at high temperature [6] or in air (Glaser coupling [7] or Hay coupling [8]). Considering this limitation, Ho et al. reported the Sonogashira reaction in an atmosphere of hydrogen gas diluted with nitrogen or argon, in which efficient cross-coupling product was formed [9]. Under this condition the side product due to terminal acetylene can be reduced to nearly 2%. Although, the exact role of hydrogen was not known, it was assumed that it may reduce O_2 in the presence of nascent Pd(0) to form water and decreases its concentration during the reaction [10]. Thus, a reducing atmosphere which controls the excessive paramagnetic oxygen may lower the acetylene homodimers and enhance the cross-coupling reaction [11]. Therefore, a high level of efficiency could be achieved by using preformed Pd(0) catalyst, or more precisely a Pd(0) nanoparticle (Pd NPs) as catalyst [12]. However in majority of cases, synthesis of Pd NPs requires high temperature, sonication and additional stabilizer, thereby making the process tedious and lengthy [13]. The development of process to prepare Pd NPs in minimum step with reducing agent from renewable sources has emerged to be the growing interest as it serves to be green and eco-friendly alternative with least chemical waste [14].

So, in this section we have utilized a non-toxic naturally abundant phytochemical, gallic acid for *in situ* generation of Pd NPs and its catalytic potential was examined in Sonogashira cross-coupling of aryl halides and terminal acetylene [14]. It is an easily available laboratory chemical which is inexpensive and possesses great antioxidant potential. The formation of the Pd NPs was confirmed by performing UV/Vis spectroscopy, Fourier Transformation Infrared Spectroscopy (FTIR), powder XRD analysis and their size and morphology were determined by Transmission Electron Microscopy (TEM).

4.1.2. Experimental

4.1.2.1. General procedure for Sonogashira cross-coupling reaction

In a 50 mL round bottom flask, a mixture of aryl halide (0.5 mmol), terminal alkyne (0.65 mmol), $Pd(OAc)_2$ (1 mol%), gallic acid (1 mol%) and K_2CO_3 (1.5 mmol) in 4 mL EtOH was stirred at 40 °C. After completion (vide TLC); the reaction mixture was diluted with H_2O and extracted with ethyl acetate (3×10 mL), dried over Na_2SO_4 and concentrated in vacuo. The residue was purified by column chromatography on silica gel using n-hexane as eluent to give corresponding functionalized alkyne. Purity of isolated product was confirmed by performing ^1H and ^{13}C NMR spectroscopy.

For reusability experiment, after the first catalytic cycle the reaction mixture was extracted with ethyl acetate and centrifuged. The organic fraction was removed for purification and the recovered residue was washed with EtOH and directly used for further catalytic cycle by the addition of fresh reactants.

4.1.2.2. General procedure for preparation of Pd NPs by *ex situ* method

In a 25 mL round bottomed flask, equimolar ratio of $Pd(OAc)_2$ (5 mg) and gallic acid (5 mg) were mixed in EtOH (4 mL) and stirred at room temperature under aerobic conditions. Instant change in colour of the resulting solution from orange to black was observed. This indicates the reduction of Pd(II) ions to nano sized Pd(0) particles. The resulting black residue was separated through centrifugation and washed with EtOH and dried under vacuum.

4.1.3. Results and Discussion

4.1.3.1. Optimization of catalytic system for Sonogashira coupling reaction

At the onset, to examine the effectiveness of gallic acid in Sonogashira reaction, we have performed the reaction using 4-iodonitrobenzene (0.5 mmol) and phenylacetylene (0.75 mmol) in presence K_2CO_3 and $Pd(OAc)_2$ (1 mol%) with gallic acid (1 mol%) in EtOH (Table 4.1.1). At room temperature the reaction proceeds with the formation of 85% isolated product (Table 4.1.1, entry 1). The formation of the diarylalkyne was confirmed by its ^1H and ^{13}C NMR spectra. From the ^1H NMR spectra, a doublet peak was observed in the downfield region (δ 8.21 ppm) corresponding to two aromatic protons, which is due to presence of adjacent $-NO_2$ group. Further, peaks at δ ppm 7.66 (d, 2H), 7.58-7.52 (m, 2H) and 7.38 (dd, 3H) corresponds to other aromatic protons. The structure was further confirmed by its ^{13}C NMR data with peaks at 94.8 and 87.6 for two

acetylene carbon and peaks at δ ppm 147.0, 132.3, 131.9, 130.3, 129.3, 128.6, 123.7, 122.1 due to aromatic ring carbon.

Table 4.1.1: Screening of catalytic effect on Sonogashira coupling [a]

Entry	Catalyst (mol%)	Gallic acid (mol%)	Time (h)	Yield (%) [b]
1	Pd(OAc)$_2$ (1)	1	5	85 [c]
2	Pd(OAc)$_2$ (1)	1	5	95
3	Pd(OAc)$_2$ (0.5)	1	7	60
4	Pd(OAc)$_2$ (1)	2	7	65
5	Pd(OAc)$_2$ (1)	5	7	50
6	-	1	24	-
7	Pd(OAc)$_2$ (1)	0.5	12	50
8	Pd(OAc)$_2$ (1)	-	12	50
9	PdCl$_2$ (1)	1	6	70
10	Pd NPs (preformed)		5	93

[a] Reaction conditions: 4-iodonitrobenzene (0.5 mmol), phenylacetylene (0.75 mmol), K$_2$CO$_3$ (1.5 mmol), EtOH (4 mL) at 40 °C. [b] Isolated yield, [c] rt
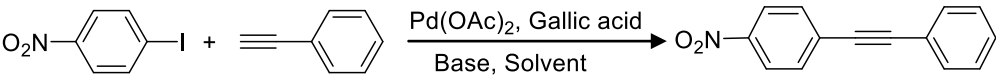
On increasing the temperature to 40°C, the reaction delivers 95% coupling product (Table 4.1.1, entry 2). By lowering the Pd loading to 0.5 mol%, poor conversion was observed and no improvement was noticed even on increasing the reaction time to 7 h (Table 4.1.1, entry 3). Optimization results showed nearly a quantitative formation of the cross-coupling product with equimolar loading of Pd(OAc)$_2$ and gallic acid (*i.e.* 1 mol%) under an environmentally preferred alcoholic reaction medium (Table 4.1.1, entry 2). Higher amount of gallic acid loading decreases the reaction progress significantly (Table 4.1.1, entries 4 and 5). High gallic acid loading prevents the increase in the size of Pd NPs, because excess reducing agent diminishes the Ostwald ripening process [15,16] by capping most of the free Pd surface sites and lowers the accessibility of the Pd particle at the surface for catalysis. When the reaction was performed in absence of Pd(OAc)$_2$, no conversion was noticed, signifying its importance as catalytic species (Table 4.1.1, entry 6). With lower amount or in absence of gallic acid, the reaction provides lower yield of desired product (Table 4.1.1, entries 7 and 8). Again with other palladium source for example PdCl$_2$, a comparatively lower efficiency was noticed (Table 4.1.1, entry 9). This may be due to different coordinating ability of anions to the nanoparticle surface (OAc$^-$ > Cl$^-$). The weaker coordination of chloride ion to Pd surface compared to acetate ion, decreases the stability of Pd NPs. This enhances the rate of palladium leaching and thus

lowers the reaction activity [17]. We have also carried out the reaction using *ex situ* prepared Pd NPs, and the cross-coupling reaction affords identical reactivity as of *in situ* condition (Table 4.1.1, entry 10).

4.1.3.2. Optimization of solvent and base for Sonogashira coupling reaction

Next, we have investigated the effect of different solvents on the catalytic system (Table 4.1.2). The catalytic activity of the *in situ* generated Pd NPs was studied in water and aqueous alcoholic solvents (1:1). The reaction efficiency decrease drastically and lower conversion was observed even under prolonged reaction time (Table 4.1.2, entries 1-3). This discrepancy is may be due to the poor interactions between the low-polar reactants and active catalyst, which may form clusters during the reaction. It is seen that the reaction proceeds efficiently in EtOH providing excellent isolated yield, however in case of *i*-PrOH lower conversion was observed (Table 4.1.2, entries 4 and 5).

Table 4.1.2: Screening the solvent and base [a]

$$O_2N-\text{(C}_6\text{H}_4\text{)}-I \ + \ \equiv-\text{(C}_6\text{H}_5\text{)} \xrightarrow[\text{Base, Solvent}]{\text{Pd(OAc)}_2, \text{Gallic acid}} O_2N-\text{(C}_6\text{H}_4\text{)}-\equiv-\text{(C}_6\text{H}_5\text{)}$$

Entry	Solvent (mL)	Base (mmol)	Time(h)	Yield (%) [b]
1	H_2O	K_2CO_3 (1.5)	23	50
2	$EtOH/H_2O$	K_2CO_3 (1.5)	12	60
3	i-PrOH/H_2O	K_2CO_3 (1.5)	12	50
4	EtOH	K_2CO_3 (1.5)	5	95
5	i-PrOH	K_2CO_3 (1.5)	9	40
6	EtOH	K_2CO_3 (1)	6	60
7	EtOH	K_2CO_3 (2)	6	85
8	EtOH	NaOAc (1.5)	6	40
9	EtOH	Cs_2CO_3 (1)	3	97
10	EtOH	NaOH (1.5)	7	30
11	EtOH	Na_2CO_3 (1.5)	8	40

[a] Reaction conditions: 4-iodonitrobenzene (0.5 mmol), phenylacetylene (0.65 mmol), Pd(OAc)$_2$ (1 mol%), gallic acid (1 mol%), solvent (4 mL) at 40 °C. [b] Isolated yield.

Since, a well chosen base is often significant for the success of the cross-coupling reaction; we next studied the role of a number of bases under optimized reaction condition. The reaction was performed using different amount of K_2CO_3, and 1.5 mmol was found to be the appropriate proportion for the cross-coupling reaction (Table 4.1.2, entries 4 vs 6 and 7). Considering these conditions, activity of various bases such as K_2CO_3, NaOAc, Cs_2CO_3, NaOH and Na_2CO_3 were studied, best result was obtained

using Cs_2CO_3 (1 mmol) in ethanol at 40 °C with Pd loading (1 mol%) within 3 h (Table 4.1.2, entries 9 vs 8, 10 and 11).

4.1.3.3. Characterization of the catalytic system

To verify the reducing role of gallic acid in the formation of Pd NPs, we have performed the UV/Vis spectroscopic analysis of the *ex situ* prepared Pd NPs and compared with the UV absorption spectra of precursor $Pd(OAc)_2$ and gallic acid solution (Figure 4.1.1, I). A peak at 259 nm was observed which corresponds to the absorption of gallic acid. The disappearance of a peak at 281 nm, due to $Pd(OAc)_2$ after addition of gallic acid, indicates the loss of acetate ion. Moreover, appearance of a characteristic absorption peak at 361 nm attributes the formation of Pd(0) particles.
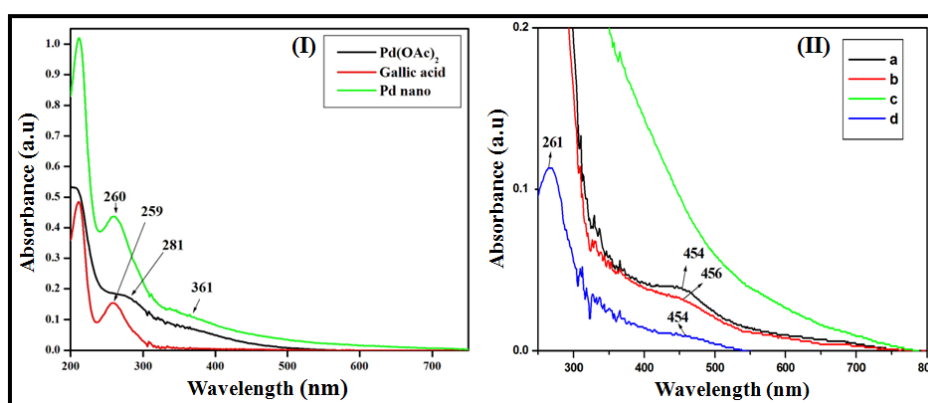
Figure 4.1.1: (**I**) UV/Vis absorption spectra of $Pd(OAc)_2$, gallic acid and preformed Pd NPs (**II**) UV/Vis absorption spectra *in situ* Pd NPs: (**a**) 1 mol% $Pd(OAc)_2$ and 1 mol% gallic acid; (**b**) 1 mol% $Pd(OAc)_2$ and 1 mol% gallic acid after 2 h; (**c**) 1 mol% $Pd(OAc)_2$ and 0.5 mol% gallic acid; (**d**) 1 mol% $Pd(OAc)_2$ and 4 mol% gallic acid.

Further, to convey the complete reduction and control the size of the particle, UV/Vis spectra at different concentration of gallic acid was taken (Figure 4.1.1, II). From the UV/Vis spectroscopic experiment, a peak at 454 nm was observed using gallic acid (1 mol%) and $Pd(OAc)_2$ (1 mol%) indicating the complete reduction of Pd(II) ion to Pd(0) (Figure 4.1.1, IIa). The UV absorption spectra after 2 h of the reaction mixture do not show any characteristic change, indicating the complete reduction of Pd(II) (Figure 4.1.1, IIb). However, no distinct absorption peak near 400 nm was observed in UV spectrum Figure 4.1.1, IIc, this may be due to the partial reduction of Pd(II) with lower gallic acid loading, which results in the disappearance of peak at 281 nm due to $Pd(OAc)_2$ but does not show any characteristic absorption for formation of Pd(0).

Furthermore, on increasing the concentration of gallic acid no significant difference in UV spectra was observed (Figure 4.1.1, IId).

The Powder XRD analysis of the Pd NP shows the formation of the face-centered cubic (fcc) lattice system of the palladium nanostructure which matches well with the standard XRD database (JCPDS card no. 89-4897) (Figure 4.1.2, I). The diffraction peak observed at 40.11°, 46.66° and 68.12° corresponds to (111), (200) and (220) reflections respectively. The reduction of Pd(II) ions was further confirmed by FTIR analysis (Figure 4.1.2, II). Infrared spectra of the Pd NPs were recorded by comparing against the precursor $Pd(OAc)_2$ as shown in Figure 4.1.2, II. The peaks at 1570 cm^{-1} is due to the C=O asymmetric stretching and C=O symmetric stretching. The sharp peak at 1424 cm^{-1} is due to the ionised carboxylate group, which disappeared after the addition of gallic acid to $Pd(OAc)_2$. The shifting of vibrational peak from 1602 cm^{-1} due to $Pd(OAc)_2$ to 1611 cm^{-1} and disappearance of vibrational mode at 691 cm^{-1} due to Pd-O signifies the perfect interaction between gallic acid and Pd(II) ions.
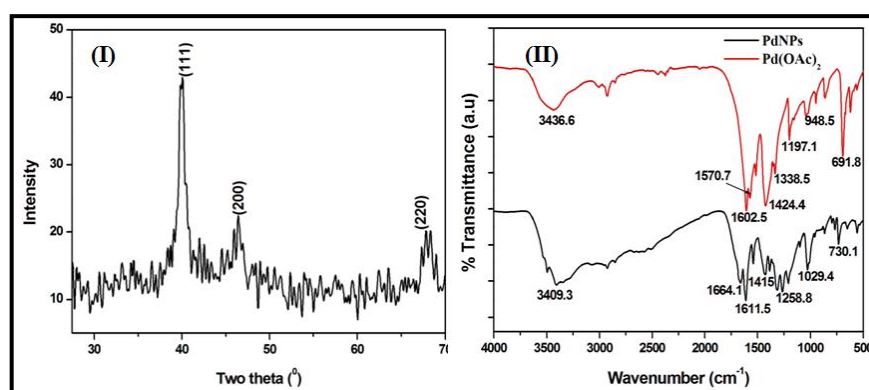
Figure 4.1.2: (**I**) Powder XRD pattern of Pd NPs, (**II**) FT-IR spectra of $Pd(OAc)_2$ and Pd NPs

It is well established from the above analysis and also from the literature that well dispersed Pd NPs are formed from Pd(II) with gallic acid where it acts as both reductant and stabilizer [18,19]. In order to further clarify the active species in the present Sonogashira reaction, Transmission electron microscope (TEM) was used and identified the size and distribution of Pd NPs (Figure 4.1.3). It was observed that the Pd NPs were well fabricated and is average dimension of 9.69 nm after 10 minute of the reaction. The selected-area electron diffraction (SAED) pattern shows five bright well resolved rings which corresponds to the reflections (111), (200) and (220) of face-centered cubic (*fcc*) Pd nanostructure. This result is consistent with the Powder XRD analysis of the Pd NPs.
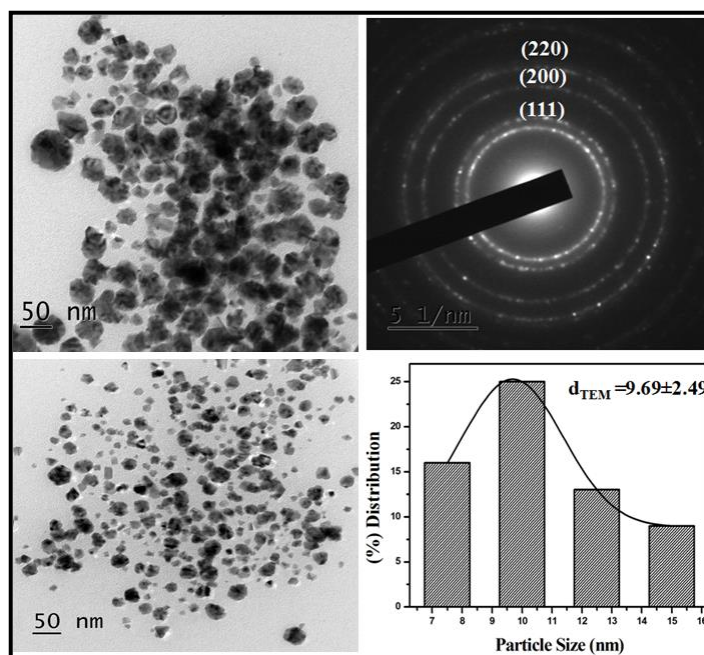
Figure 4.1.3: TEM images of gallic acid derived *in situ* generated Pd NPs

The stabilization of Pd NPs by gallic acid is thought to be due to the high anionic charge of the gallate ions [20,21]. Thus, the active catalytic species of the reaction might be the *in situ* formed Pd NPs. To identify the true active catalytic species, we have performed the mercury-poisoning test [22,23]. For this, gallic acid and Pd(OAc)$_2$ were stirred in EtOH containing Cs$_2$CO$_3$ and excess of Hg(0) (molar ratio to [Pd] ~400) for 30 min prior to addition of the reacting substrates. After 3 hours of addition of the reactants, negligible amount of coupling product formation was observed. This suggested that the Pd NPs are acting as a true heterogeneous catalyst, and the reaction is occurring on the molecular surface.

4.1.3.4. Mechanism of generation of Pd NPs

Various studies have been done to identify the anti-oxidizing characteristics of gallic acid. In general, phenolic acids can act as antioxidants either by donating a hydrogen atom or by acting as electron donors [24]. In this case, gallic acid acts as an efficient electron-proton donor species and represents a redox system via oxidation to dehydrogallic acid and reduction of Pd(II) species to Pd(0) [20] (Scheme 4.1).

(I)

Gallic acid

Dehydrogallic acid

(II)

$$Pd(II) + 2e^- \longrightarrow Pd(0)$$
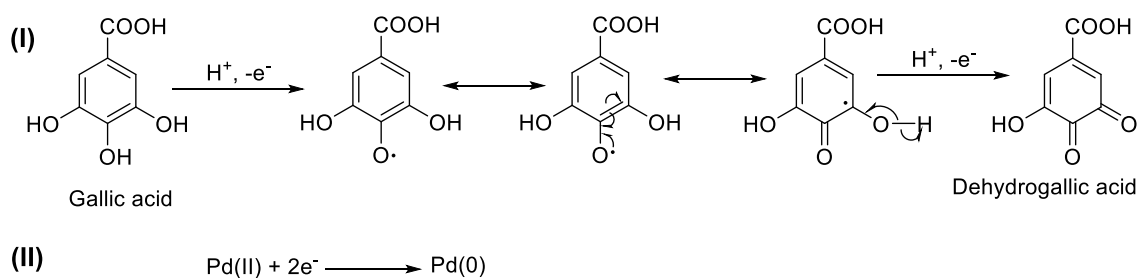
Scheme 4.1.1: Mechanism of reducing action gallic acid for *in situ* generation of Pd NPs.

4.1.3.5. Substrate scope for Sonogashira coupling reaction

Finally, to probe the scope of the catalytic system using our standard reaction conditions, we have evaluated various aryl halides and terminal alkynes (Table 4.1.3).

Table 4.1.3: Substrate scope of Sonogashira coupling [a]

Entry	X	R^1	R^2	Time(h)	Yield(%) [b]
1	I	4-NO$_2$	C$_6$H$_5$	3	97
2	Br	H	C$_6$H$_5$	7	70
3	Br	H	C$_6$H$_5$	4	95 [c]
4	Br	4-CH$_3$	C$_6$H$_5$	6	80 [c]
5	Br	4-NO$_2$	C$_6$H$_5$	6	65 [c]
6	I	3-NO$_2$	C$_6$H$_5$	4	92
7	I	4-Me	C$_6$H$_5$	3	98
8	I	4-Me	4-MeC$_6$H$_4$	4	95
9	I	3-Me	C$_6$H$_5$	4	95
10	I	4-OMe	C$_6$H$_5$	4	80
11	I	H	C$_6$H$_5$	3	98
12	I	H	4-MeC$_6$H$_4$	5	97
13	I	2-NO$_2$	C$_6$H$_5$	8	40
14	I	H	*n*-octyl	5	80
15	I	H	*n*-butyl	5	85
16	I	H	cyclohexyl	5	90
17	I	4-Me	*n*-butyl	5	80
18	I	3-Iodopyridine	C$_6$H$_5$	12	90
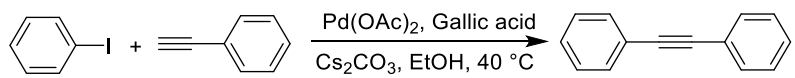
[a] Reaction conditions: aryl halide (0.5 mmol), acetylene (0.65 mmol), Pd(OAc)$_2$ (1 mol%), gallic acid (1 mol%), Cs$_2$CO$_3$ (1 mmol), EtOH (4 mL) [b] Isolated yield, [c] at 60 °C

The reaction system is compatible with a wide array of electronically diverse substituents. When investigating the influence of the nature of the halide (Table 4.1.3, entries 1-5), as predicted a slight decrease in conversion was observed when going from iodide to bromide. In case of bromide, an increase in the reaction temperature improves the conversion with low reaction time. However, substitution at *para*-position lowers the reaction yield even when the reaction time was increased to six hours (Table 4.1.3, entries 4, 5). We evaluated coupling of different substituted aryl iodide with acetylene (Table 4.1.3, entries 6-17). Aryl iodides possessing an electron withdrawing group (*e.g.* NO_2) at *para*- or *meta*-position affords improved yield on coupling with phenyl acetylene (Table 4.1.3, entry 1 and 6). Conversions were always complete for *para*- and *meta*-substituted derivatives (Table 4.1.3, entries 1 and 6-10), but decreased efficiency was observed for 2-iodonitrobenzene, probably due to steric hindrance (Table 4.1.3, entry 13). The effectiveness of the present protocol was also studied for aliphatic alkynes in which moderate to high yield of cross-coupling products was observed in all cases (Table 4.1.3, entries 14-17). Again the reaction provides excellent yield using heteroaryl iodide and phenylacetylene as coupling partners (Table 4.1.3, entry 18).

4.1.3.6. Catalyst reusability

From the green chemistry perspectives, the major challenges of a metal catalyst are its ability for recycling without significant loss in activity and efficiency. Considering this, the reusability of the *in situ* derived Pd NPs was investigated by consecutive Sonogashira coupling reactions of iodobenzene (2 mmol) and phenylacetylene (1.3 mmol) (Table 4.1.4).

Table 4.1.4: Reusability of the *in situ* generated Pd NPs in Sonogashira coupling [a]

Entry	Run	Time (h)	Yield (%) [b]
1	1	3	98
2	2	3	96
3	3	4	89
4	4	5	86

[a] Reaction conditions: iodobenzene (1 mmol), acetylene (1.3 mmol), Pd(OAc)$_2$ (1 mol%), gallic acid (1 mol%), Cs$_2$CO$_3$ (1 mmol), EtOH (4 mL) [b] Isolated yield

After the first catalytic cycle, the diarylalkyne was easily isolated by extraction with ethyl acetate and the catalytic species was recovered for the next catalytic run. The

recovered residue was directly used without further modification followed by addition of fresh reactants. Identical results were obtained upto 2nd run, thereafter a slight loss in activity was observed in 3rd and 4th cycles. We have performed powder XRD analysis of the Pd NPs after 1st catalytic run and the diffraction peaks are observed at 40.11° and 46.66° which corresponds to (111) and (200) reflections respectively, with face-centered cubic (*fcc*) lattice system of the Pd NPs according to JCPDS card no. 89-4897 (Figure 4.1.4 a). Thereafter, TEM image showed that the size of NPs get reduced after 2nd catalytic cycle with the average particle size distributions of 4.7 nm of the Pd NPs (Figure 4.1.4 b & d). Selected-area electron diffraction (SAED) pattern distinctly shows the presence of (111) and (220) crystal planes (Figure 4.1.4 c). The decrease in size of the Pd NPs after consecutive run could be due to the aggregation and precipitation of the large sized NPs, which leaves smaller particles in solution [16]. This decrease of active particles may have lowered the catalytic activity of the cross-coupling reaction.
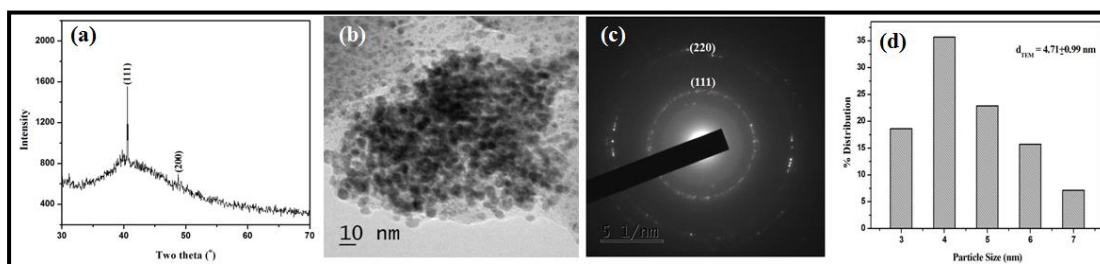
Figure 4.1.4: **(a)** Powder XRD pattern of *in situ* generated Pd NPs after 1st catalytic run **(b)**TEM images **(c)** SAED pattern and **(d)** Particle size distribution of *in situ* generated Pd NPs after 2nd catalytic run

4.1.4. Conclusions

In summary, we have developed a simple, one pot and green method for Sonogashira cross-coupling reaction using bio-friendly alternative for generation of Pd NPs. The present protocol shows an excellent study on the influence of gallic acid on the reaction rate and size distribution of Pd NPs. Moreover, the reaction is highly compatible with diverse range of functional groups for the cross-coupling reaction.

## 4.1.5. Analytical data of the synthesized alkynyl derivatives
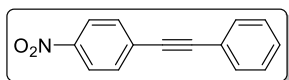
1-Nitro-4-(2-phenylethynyl)benzene (Table 4.1.3, entry 1): Yellow Solid, m.p. 119-121 °C, **^{1}H NMR (400 MHz, CDCl$_3$):** δ 8.21 (d, 2H, J = 9.0 Hz), 7.66 (d, 2H, J = 9.0 Hz), 7.58-7.52 (m, 2H), 7.38 (dd, 3H, J = 5.1, 1.9 Hz) ppm. **^{13}C NMR (100 MHz, CDCl$_3$):** δ 147.0, 132.3, 131.9, 130.3, 129.3, 128.6, 123.7, 122.1, 94.8, 87.6 ppm.
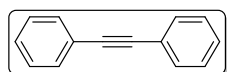

Diphenylacetylene (**Table 4.1.3, entry 3**): White Solid, .p. 54-56 °C, **^{1}H NMR (400 MHz, CDCl$_3$):** δ 7.57-7.56 (m, 4H), 7.37-7.35 (m, 6H) ppm. **^{13}C NMR (100 MHz, CDCl$_3$):** δ 131.7, 128.6, 128.4, 123.4, 89.4 ppm.
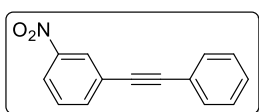
1-Nitro-3-(2-phenylethynyl)benzene (Table 4.1.3, entry 6): Yellow gum, **^{1}H NMR (400 MHz, CDCl$_3$):** δ 8.34 (s, 1H), 8.17 (d, 1H, J = 8.2 Hz), 7.81 (d, 1H, J = 7.3 Hz), 7.56-7.50 (m, 3H), 7.37-7.24 (m, 3H) ppm. **^{13}C NMR (100 MHz, CDCl$_3$):** δ 137.3, 131.9, 129.4, 129.2, 128.6, 126.5, 125.3, 122.9, 122.3, 92.0, 86.9 ppm.
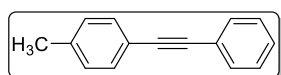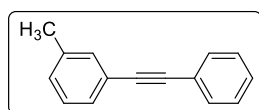

1-Methyl-4-(2-phenylethynyl)benzene (Table 4.1.3, entry 7): White solid, m.p. 68-70 °C, **^{1}H NMR (400 MHz, CDCl$_3$):** δ 7.52-7.50 (m, 2H), 7.41 (d, 2H, J = 8.2 Hz), 7.34-7.31 (m, 3H), 7.14 (d, 2H, J = 8.2 Hz), 2.36 (s, 3H) ppm. **^{13}C NMR (100 MHz, CDCl$_3$):** δ 138.4, 132.5, 131.6, 129.3, 128.5, 128.1, 123.5, 120.2, 89.6, 88.7, 21.6 ppm.
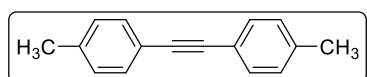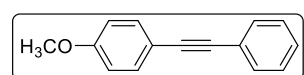

1-Methyl-4-[2-(*p*-tolyl)ethynyl]benzene (Table 4.1.3, entry 8), White solid, m.p. 126-128 °C, **^{1}H NMR (400 MHz, CDCl$_3$):** δ 7.40 (d, 4H, J = 7.8 Hz), 7.13 (d, 4H, J = 8.2 Hz), 2.35 (s, 6H) ppm. **^{13}C NMR (100 MHz, CDCl$_3$):** δ 138.2, 131.5, 129.2, 120.4, 88.9, 87.2, 21.5 ppm.


1-Methyl-3-(2-phenylethynyl)benzene (Table 4.1.3, entry 9): Colourless liquid, **^{1}H NMR (400 MHz, CDCl$_3$):** δ 7.53-7.51 (m, 2H), 7.36-7.33 (m, 4H), 7.25-7.21 (m, 2H), 7.14 (d, 1H, J = 7.3 Hz), 2.35 (s, 3H) ppm. **^{13}C NMR (100 MHz, CDCl$_3$):** δ 138.1, 134.5, 132.6, 131.7, 129.3, 128.8, 128.4, 128.3, 123.5, 123.2, 89.7, 89.2, 21.4 ppm.
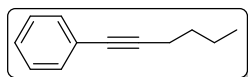

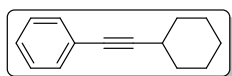**1-Methoxy-4-(2-phenylethynyl)benzene (Table 4.1.3, entry 10):** White solid, m.p. 79-81 °C, **^{1}H NMR (400 MHz, CDCl$_3$),** δ 7.51-7.44 (m, 4H), 7.32-7.30 (m, 3H), 6.86 (d, J = 8.7 Hz, 2H), 3.82 (s, 3H) ppm **^{13}C NMR (100 MHz, CDCl$_3$):** δ 159.7, 133.1, 131.5, 128.4, 128.0, 123.7, 115.4, 114.1, 89.9, 89.4, 55.4 ppm.
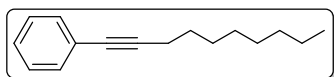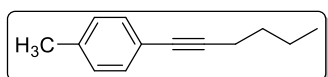
1-(Dodec-1-yn-1-yl)-benzene (Table 4.1.3, entry 14): yellow liquid; ^{1}H NMR (400 MHz, CDCl$_3$): δ 7.39-7.36 (m, 2H), 7.27-7.24 (m, 3H), 2.38 (t, 2H, J = 6.8 Hz), 1.59-1.41 (m, 12H), 0.87 (t, 3H, J = 6.8 Hz) ppm. ^{13}C NMR (100 MHz, CDCl$_3$): δ 131.6, 128.2, 127.5, 124.1, 90.5, 80.6, 32.0, 29.7, 29.4, 29.2, 28.8, 22.7, 19.4, 14.2 ppm.

**1-(Hex-1-yn-1-yl)-benzene (Table 4.1.3, entry 15)**: yellow liquid; ^{1}H NMR (400 MHz, CDCl$_3$): δ 7.40-7.38 (m, 2H), 7.27-7.25 (m, 3H), 2.41 (t, 2H, J = 6.8 Hz), 1.60-1.45 (m, 4H), 0.94 (t, 3H, J = 7.3 Hz) ppm. ^{13}C NMR (100 MHz, CDCl$_3$): δ 131.6, 128.2, 127.5, 124.1, 90.5, 80.6, 29.7, 22.0, 19.1, 13.7 ppm.

1-(Cyclohexylethynyl)benzene (Table 4.1.3, entry 16): Yellow liquid, ^{1}H NMR (400 MHz, CDCl$_3$): δ 7.39-7.37 (m, 2H),, 7.29-7.24 (m, 3H), 2.57-2.56 (m, 1H), 1.88-1.48 (m, 10H) ppm. ^{13}C NMR (100 MHz, CDCl$_3$): δ 131.6, 128.2, 127.4, 124.2, 94.5, 80.5, 32.8, 29.7, 26.0, 24.9 ppm.

1-(Hex-1-yn-1-yl)-4-methylbenzene (Table 4.1.3, entry 17): Yellow liquid, ^{1}H NMR (400 MHz, CDCl$_3$): δ 7.35 (d, 1H, J = 8.2 Hz), 7.29-7.06 (m, 3H), 2.36 (s, 3H), 1.59-1.56 (m, 2H), 1.49-1.31 (m, 4H), 0.96-0.92 (m, 3H) ppm. ^{13}C NMR (100 MHz, CDCl$_3$): δ 137.4, 131.4, 129.1, 128.7, 100.0, 87.2, 31.0, 29.7, 22.9, 19.2. 13.6 ppm.
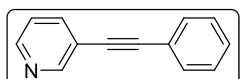
3-(Phenylethynyl)pyridine (Table 4.1.3, entry 18): Yellow liquid, ^{1}H NMR (400 MHz, CDCl$_3$): δ 8.79-8.78 (m, 1H), 8.56 (dd, 1H, J = 4.9, 1.7 Hz), 7.87-7.78 (m, 1H), 7.60-7.48 (m, 2H), 7.43-7.23 (m, 4H).ppm. ^{13}C NMR (100 MHz, CDCl$_3$): δ 152.2, 148.5, 138.4, 131.7, 131.6, 128.8, 128.4, 123.0, 122.4, 92.6, 85.9 ppm.

^{1}H and ^{13}C NMR spectra of 1-Methyl-4-[2-(p-tolyl)ethynyl]benzene
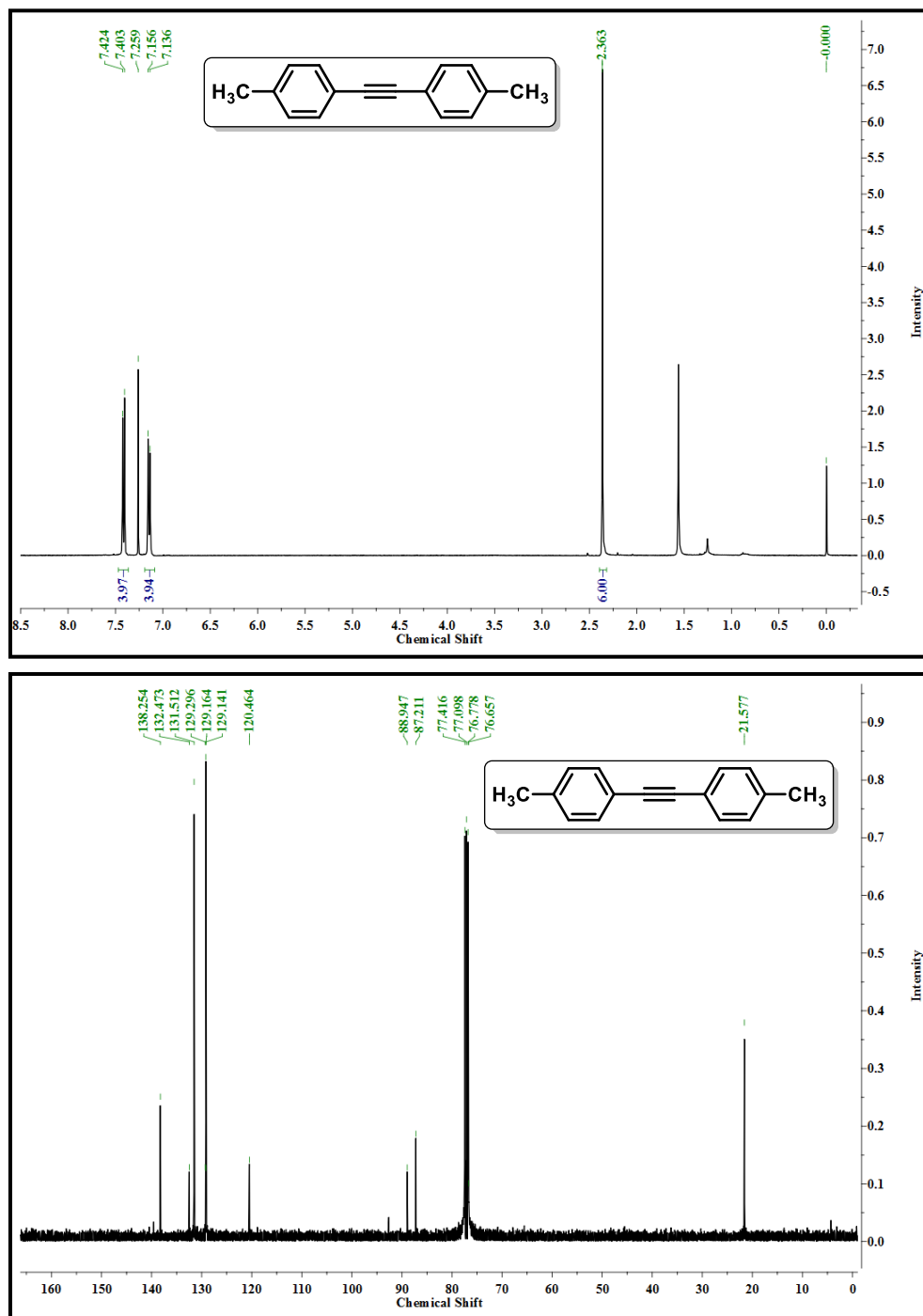
Section 4.2

Application of plant extract towards NOSE approach: A comparative study of catalytic activity in C_{sp2}-C_{sp2} and C_{sp2}-C_{sp} cross-coupling reaction

Abstract: This section discloses the use of plant extract as reducing and stabilizing agents for generation of Pd NPs. Comparative studies have been done on the activity of two plant species (*Ocimum santum and Aloe vera*) in generation of palladium nanoparticles via *ex situ* and *in situ* method. The catalytic activity of both the *in situ* and *ex situ* condition was examined in Suzuki-Miyaura and Sonogashira cross-coupling reaction.

4.2.1. Introduction

In recent years, metal nanoparticles (NPs) have found wide application in catalysis and biomedical diagnostics due to their unique size, shape and composition. These materials are susceptible to various chemical and physical modifications and can conjugate with varying antibodies, ligands and drugs providing wide range of potential applications [25-28]. Nowadays catalytic activity of metal NPs finds wide application in organic synthesis. In this respect, "NOSE" (nanoparticle-catalyzed organic synthesis enhancement) approach is considered as an effective route for various organic transformations [29,30]. Various chemical, physical, and biological methods have been explored for synthesis of metal NPs [31,32]. Chemical and physical methods for generation of NPs are associated with toxic by-products, laborious experimental techniques and uneconomical issues. As such, introduction of microorganism or plant resources provides an environmentally benign and cost effective alternative route for the synthesis of metal NPs [33-35]. Plant extracts posses various biologically active phytochemicals (e.g alkaloids, terpenoids, polyphenolic compounds.) which itself serve as a reducing/stabilizing agent for bulk transition metals to nano-dimensional particles [34]. Plant-based approach for synthesis of metal NPs not only provides faster rate of reduction of metal ions but nucleate/cap them into stable and controlled morphology. As such biogenic reduction of metal ions in absence of chemical reagents is an interesting approach on account of the environmental sustainability.

Of all the transition metals, palladium contributes an impressive ability to construct C-C bonds between diverse functionalized substrates [36]. So, in this section we present a comparative study of two plant extracts (*Ocimum santum and Aloe vera*) in synthesis of Pd NPs and their catalytic activity was examined in Suzuki-Miyaura and Sonogashira cross coupling reactions via both the *ex situ* and *in situ* method.

4.2.2. Experimental

4.2.2.1. Procedure for isolation of plant extracts

Preparation of Ocimum sanctum leaf extract (Ext OS): 1g of fresh leaves of *Ocimum sanctum* was collected and washed thoroughly with distilled water and grinded in a mortar. The pastes so obtained were transferred to a 50 mL beaker and mixed with 10 mL distilled water. The resulting mixture was then boiled for 5 minutes. The mixture was allowed to cool and the filtrate was separated and collected for further use [37].

Preparation of Aloe vera Extract (Ext AV): 10g of healthy leaves of *Aloe vera* were collected and washed thoroughly with distilled water. The leaves were squeezed to extract the gel and collected in a beaker. The mixture was sonicated for 30 minutes to obtain the uniform gel type extract and then stored in the refrigerator for further use.

4.2.2.2. General method of preparation of Pd NPs by *ex situ* method

2 mL 0.05 N (0.01 g) alcoholic $Pd(OAc)_2$ was mixed with 4 mL of the respective aqueous extract and stirred at room temperature. The mixture of $Pd(OAc)_2$/extract solution show a gradual change in colour after specific time interval, indicating the reduction of Pd(II) ion. The resulting Pd NPs were separated through centrifugation and washed with EtOH and acetone in sequence. Thereafter the pastes were dried under vacuum and stored for further analysis.

4.2.2.3. Experimental procedure for the catalytic reactions

(A)Typical procedure for in situ catalyzed Suzuki-Miyaura reaction: A mixture of aryl halide (0.5 mmol), aryl boronic acid (0.6 mmol), K_2CO_3 (1.5 mmol), $Pd(OAc)_2$ (1 mol%), required amount of extract and EtOH: H_2O (1:1) were taken in a 25 mL round-bottom flask. The reactants were allowed to stir at room temperature. The progress of the reaction was monitored vide TLC. After completion, the catalyst was separated from the reaction mixture by centrifugation and the crude reaction mixture was extracted with ethyl acetate (3×10 mL). The resultant organic fraction was washed with brine (2×10 mL) and dried over anhydrous Na_2SO_4 and evaporated under reduced pressure. The desired product was isolated by column chromatography using ethyl acetate and hexane as an eluent and purity was confirmed by ^{1}H and ^{13}C NMR spectroscopic analyses.

(B)Typical procedure for in situ catalyzed Sonogashira coupling reaction: In a 50 mL round bottom flask $Pd(OAc)_2$ (1 mol% ,0.001g) and required amount of extract was mixed. To the resulting mixture, aryl halide (0.5 mmol) and terminal alkyne (0.6 mmol) was added followed by addition of EtOH (4 mL) and K_2CO_3 (1.5 mmol). The mixture was then stirred at 40°C and the progress of the reaction was monitored by TLC. After completion, the reaction mixture was diluted with H_2O and extracted with ethyl acetate (3×10 mL), dried over Na_2SO_4 and concentrated in vacuum. The residue was purified by column chromatography on silica gel using n-hexane as eluent to obtain the pure product (functionalized alkyne). Purity of isolated products was confirmed by ^{1}H and ^{13}C NMR spectra.

(C) Catalytic procedure using Pd NPs$_{ex\text{-}situ}$ prepared from respective Ext OS (Pd$_{OS}$ NP) and Ext AV(Pd$_{AV}$ NP): In two separate 50 mL round bottom flask, Pd NPs (1 mol%) was mixed with aryl halide (0.5 mmol) and aryl boronic acid (0.6 mmol)/phenylacetylene (0.6 mmol) respectively with K$_2$CO$_3$(1.5 mmol) in required amount of solvent. The reaction mixtures were allowed to stir at room temperature and 40°C respectively. The progress of both the coupling reaction Suzuki-Miyaura and Sonogashira, were monitored via TLC and desired product was isolated by column chromatographic technique using n-hexane as eluent.

4.2.3. Results and Discussion

4.2.3.1. Characterization of Pd NPs

During the preparation of Pd NPs it was noticed that, both the extract and Pd(OAc)$_2$ mixture undergoes reduction of Pd(II) to Pd(0) in different time intervals (Figure 4.2.1). The mixture of Pd(OAc)$_2$ and Ext OS show a gradual change in colour from brown to dark brown within 15 minutes and to complete black after 1h, indicating the reduction of Pd(II) ion (Figure 4.2.1a). However, the mixture of Pd(OAc)$_2$ and Ext AV, shows a gradual change in colour from brown to dark brown in 5 h and subsequently to black after 12h (Figure 4.2.1b).
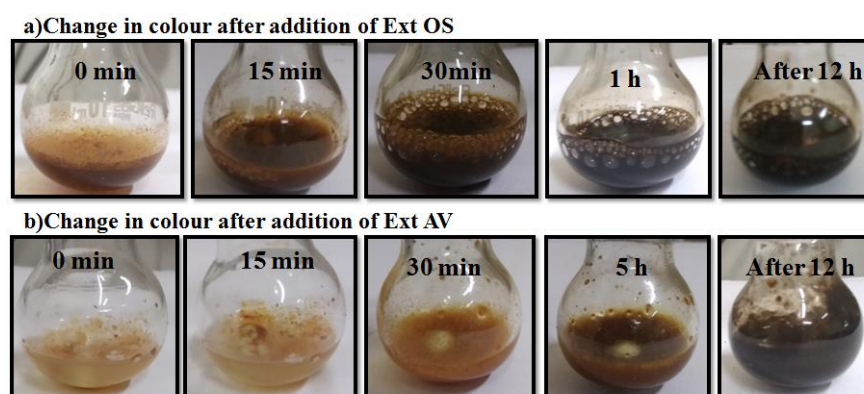

Figure 4.2.1: Change in colour of Pd(OAc)$_2$ after addition of (a) Ext OS (b) Ext AV

This difference in reducing rate of both the extracts may be due to the presence of different concentration of phytochemicals in the respective plant species. It is seen from literature studies that various quantitative analyses have been done to reveal the chemical compositions of *Ocimum sanctum* (OS*)* and *Aloe vera* (AV). From the comparative study of both the plant species it was found that *Ocimum sanctum* leave possess greater amount of reducing sugar and ascorbic acid than *Aloe vera* (Table 4.2.1) [38-41]. Hassan and

Kashif reported the presence of different amount of reducing sugar and ascorbic acid in *Ocimum sanctum*, however the composition is greater than present in *Aloe vera*. Since ascorbic acid and different reducing sugars are used in generation of NPs [42-44], these phytochemical in the respective plant species might helped in the reduction of Pd(II) ion. However, presence of greater amount of these chemical constituents in OS as compared to AV reveal its greater reducing potential. Additionally other phytochemicals such as flavanoids, essential oils and phenolic contents are also present which may also assist in the reduction/stabilization of metal NPs [45-50].

Table 4.2.1: Comparison of basic phytochemical composition of *Ocimum sanctum* and *Aloe vera*

Parameters	*Aloe vera*	*Ocimum sanctum*	
Ascorbic acid (mg/100g)	1.90 [40]	(65.41 ±0.76) [38]	(02.41±0.91) [39]
Reducing sugar (%)	0.36 [41]	(3.58±0.14) [38]	(26.52±1.54) [39]

Next, in order to confirm the formation of Pd NPs, we have performed the powder XRD of the respective prepared Pd NPs. Figure 4.2.2 a, shows the Powder XRD pattern of Pd_{OS} NP, which matches well with the standard JCPDS card no. 89-4897. The diffraction peaks at 2θ value of 40.5°, 46.3° and 67.8° corresponding to crystallographic planes (111), (200) and (220) respectively, suggesting the formation of face centered cubic (fcc) lattice system of Pd_{OS} NPs. Figure 4.2.2 b, shows the Powder XRD pattern of Pd_{AV} NPs, which shows the formation of fcc lattice system (JCPDS card no. 89-4897) with additional tetragonal system for PdO nano structure (JCPDS card no. 75-0200). The observed peaks at 2θ value of 39.9°, 46.1° and 68.3° correspond to (111), (200) and (220) reflections respectively, with two additional diffraction peaks of PdO at 2θ value of 18.1 and 30.6 for (001) and (100) reflections, respectively. The formation of Pd/PdO in case of Pd_{AV} NPs may be due to longer time requirement for reduction of Pd(II) which as a result leads to aerial oxidation of the Pd(0).
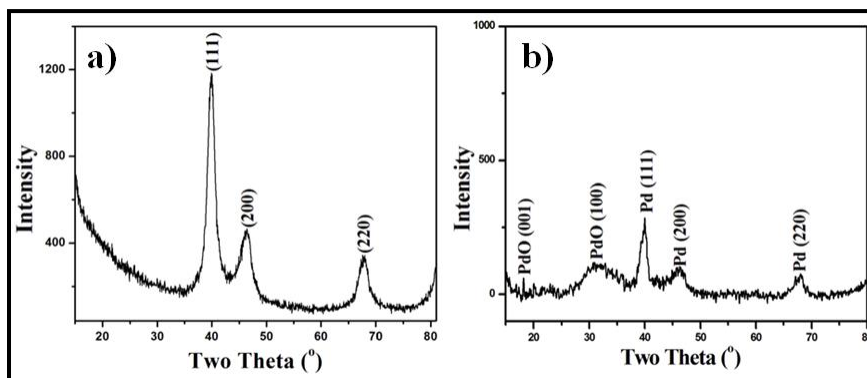
Figure 4.2.2: Powder XRD pattern of (**a**) Pd$_{OS}$ NPs and (**b**) Pd$_{AV}$ NPs

Infrared spectra of the Pd$_{OS}$ NPs and Pd$_{AV}$ NPs were recorded by comparing with the precursor Pd(OAc)$_2$ as shown in Figure 4.2.3. The shifting/disappearance of characteristic peaks of Pd(OAc)$_2$ reveals the formation of metallic Pd(0) particles. Figure 4.2.3 a, shows the vibrational peaks at 1604 cm^{-1} and 1332.2 cm^{-1} which is due to the respective asymmetric and symmetric stretching of C=O [51]. The sharp peak at 1408.5 cm^{-1} is due to the ionised carboxylate group. The shifting of these vibrational mode after the addition of Ext OS and Ext AV to Pd(OAc)$_2$ is due the ligand exchange of the corresponding ions (Figure 4.2.3 b and c). The disappearance of peak at 691.3 cm^{-1} due to Pd-O further validates the formation of Pd(0) nano structure using Ext OS [52]. In Figure 4.2.3 c, the peak in the region 781 cm^{-1} and 597 cm^{-1}, signifies the presence of PdO along with Pd(0) particles in Pd$_{AV}$ NPs.
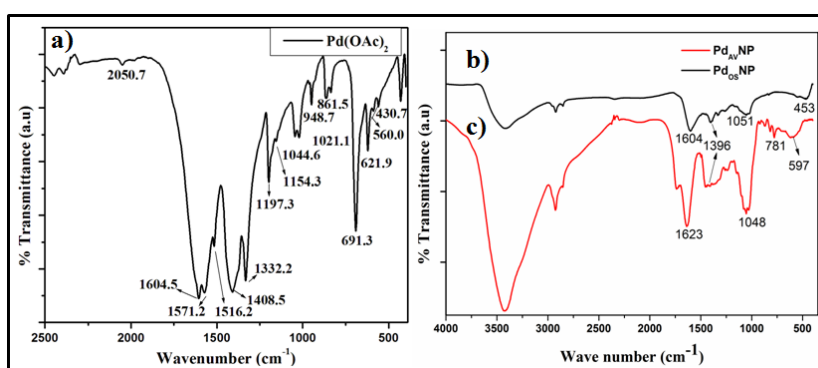

Figure 4.2.3: FT-IR spectrum of (**a**) Pd(OAc)$_2$, (**b**) Pd$_{OS}$ NPs and (**c**) Pd$_{AV}$ NPs

In order to confirm the oxidation state of palladium on Pd$_{OS}$ NPs and Pd$_{AV}$ NPs, we have characterized the synthesized NPs via XPS analysis. Figure 4.2.4 a, shows the survey scan spectrum of Pd$_{OS}$ NPs indicating the presence of Pd. The high-resolution

peak fitting spectrum of Pd_{OS} NPs comprises two peaks at 335.05 eV and 340.20 eV attributed to the $Pd3d_{5/2}$ and $Pd3d_{3/2}$ spin-orbit peaks of Pd(0) as shown in Figure 4.2.4 b. From the XPS analysis of Pd_{OS} NPs, it is evident that Pd is present in zero (0) oxidation state. However, the survey scan XPS analysis of Pd_{AV} NPs signifies the occurrence of Pd and O as shown in Figure 4.2.4 c. The high resolution peak fitting Pd3d spectrum for Pd_{AV} NPs reveals the presence of four peaks at 334.66 eV, 337 eV, 338.93 eV and 342.30 eV, which belongs to the Pd(0), Pd(II), Pd(0) and Pd(II), respectively (Figure 4.2.4 d). Therefore, the formation of Pd/PdO NPs is confirmed from the high resolution XPS spectrum. Further, the high-resolution O1s spectrum as shown in Figure 4.2.4 e also confirmed the presence of PdO in Pd_{AV} NPs.
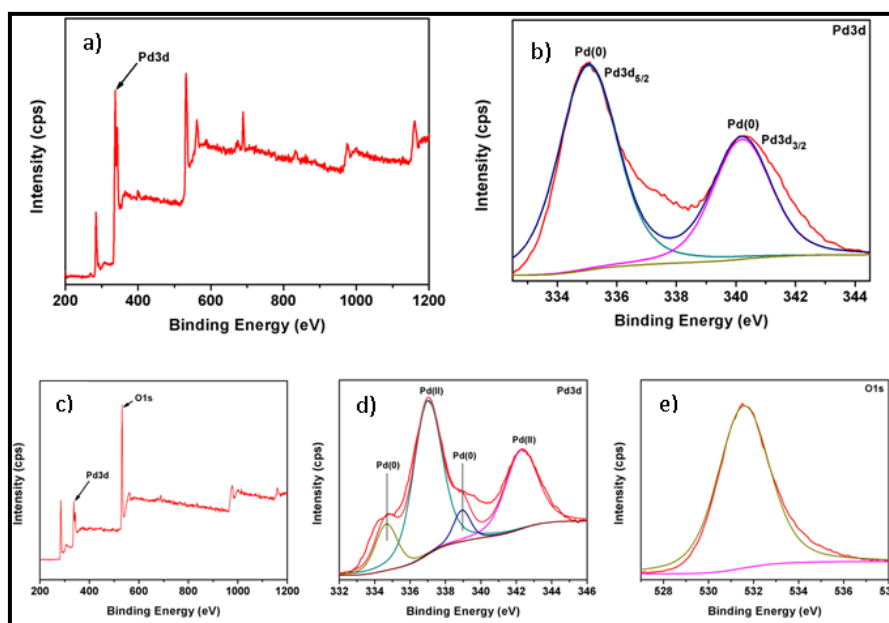

Figure 4.2.4: (a) XPS survey spectrum of Pd_{OS} NPs (b) high-resolution Pd3d spectrum of Pd_{OS} NPs (c) XPS survey spectrum of Pd_{AV} NPs (d) high-resolution Pd3d spectrum of Pd_{AV} NPs and (e) high-resolution O1s spectrum of Pd_{AV} NPs

The potential of the Ext OS and Ext AV was examined in case of *in situ* generation of NPs and the formation of Pd NPs was confirmed by UV/Vis spectroscopic experiment and TEM analyses. Figure 4.2.5 (a, b & c) shows the UV-Visible absorption spectra of the *in situ* generated colloidal suspension of Pd_{OS} NPs. A weak band at 279 nm was observed in Figure 4.2.5 a, which corresponds to Ext OS [53,54]. After the addition of $Pd(OAc)_2$, an additional peak centered near 400 nm was observed which is a characteristic of Pd(II) ion (Figure 4.2.5 b) [55]. Subsequent bio-reduction of the precursor $Pd(OAc)_2$ solution results in disappearance of the corresponding peak at 400

nm (Figure4.2.5 c), indicating the complete reduction of the Pd(II) salts to nanosized Pd(0). Figure 4.2.5 d shows a distinctive UV absorption peak at 260 nm due to $Pd(OAc)_2$ and Ext AV solution. On addition of subsequent reactants of C-C coupling the peak at 260 nm disappeared which signifies the complete reduction of Pd(II) (Figure 4.2.5 e). However, a very broad UV absorption peak centered near 260 nm was observed for pre-prepared Pd_{AV} NPs (Figure 4.2.5 f) which shows that Pd(II) ion in this condition doesn't undergo complete reduction to Pd(0) even after prolonged stirring.
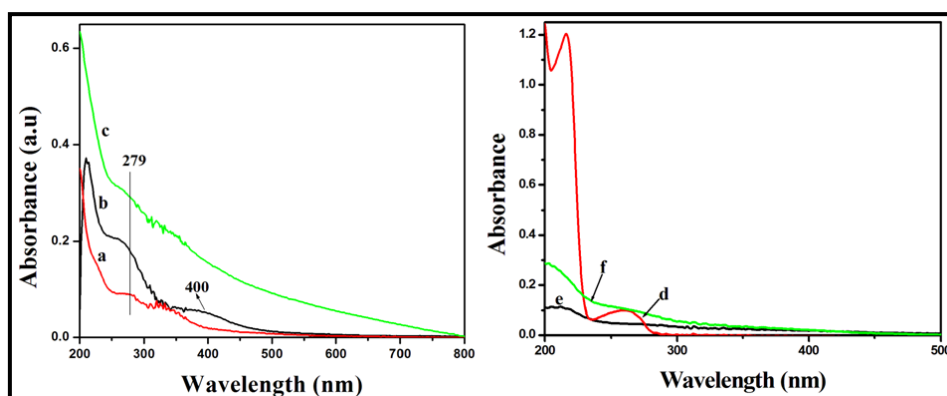

Figure 4.2.5: UV visible spectra of **(a)** Ext OS **(b)** $Pd(OAc)_2$ & Ext OS **(c)** Pd_{OS} NPs*in situ* **(d)** $Pd(OAc)_2$ & Ext AV **(e)** Pd_{AV} NPs*in situ* **(f)** Pd_{AV} NPs*ex situ*

The morphology of the *in situ* generated Pd NPs was studied by TEM imaging. It can be seen that the *in situ* generated Pd_{AV} NPs shows well dispersed spherical NPs between 4-5 nm with the interplaner distance of 0.22 nm, 0.19 nm and 0.29 nm, which corresponds to the lattice plane (111), (200) for Pd NPs and (100) for PdO respectively, Figure 4.2.6 (a, b and c). The selected area electron diffraction pattern of the Pd_{AV} NPs*in situ* shows polycrystalline fringes with four well resolved rings corresponding to crystal lattice plane namely (111), (200), (220) and (311) which agrees well with the XRD database for the fcc crystal structure of the Pd NPs as shown in Figure 4.2.6 d.

Figure 4.2.6 e, f and g, represents the HRTEM and TEM images of the *in situ* generated Pd_{OS} NPs with interplaner distance of 0.22 nm and 0.19 nm corresponding to (111) and (200) reflection respectively. The TEM images clearly reflect crystalline fringes with four well resolved rings as indexed in the selected area electron diffraction pattern of Pd NPs inset in Figure 4.2.6 f. The crystal lattice plane as depicted in the inset namely (111), (200), (220) and (222) agrees well with the XRD database for corresponding *hkl* planes which suggests the fcc crystal structure of the Pd NPs.

Additionally, it is observed that the Pd_{OS} NPs are well dispersed and spherical in shape (Figure 4.2.6 g). The distribution of the *in situ* generated Pd_{OS} NPs was analyzed using Gaussian fits (Figure 4.2.6 h) and the resultant data were plotted in a histogram showing a majority of particles being in the range of 4-5 nm, with a mean diameter of about 4.41 nm.
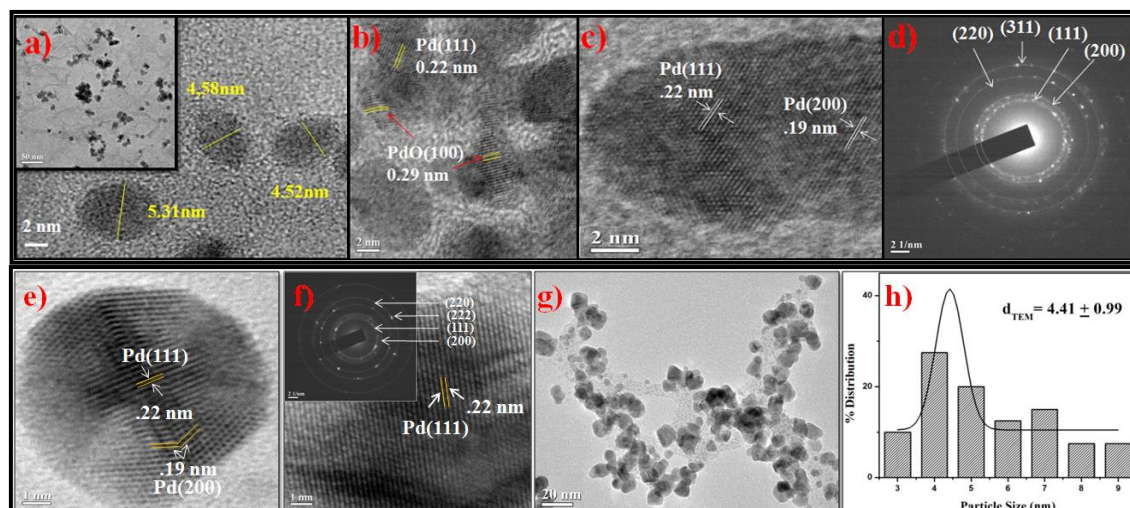

Figure 4.2.6: (**a, b, c** and **d**) are the TEM and HRTEM images and SAED pattern of the Pd_{AV} NPs*in situ*, (**e**, **f and g**) are the HRTEM images and TEM image and (**h**) is the particle size distribution of the Pd_{OS} NPs*in situ*. Inset in (**f**) is the SAED pattern of the Pd_{OS} NP *in situ*

4.2.3.2. Catalytic activity of the Pd NPs

4.2.3.2.1. Optimization of reaction conditions for Suzuki-Miyaura reaction

The catalytic activities of both the Pd NPs were investigated for the Suzuki-Miyaura cross-coupling reaction. Initially, the catalytic activity was examined for the *ex situ* prepared Pd NPs using 4-bromonitrobenzene (1 mmol) and phenylboronic acid (1.2 mmol) as the model substrate (Table 4.2.2).

The reaction affords only 30% and 10% of isolated yields of cross-coupling product with both *ex situ* generated Pd_{AV} and Pd_{OS} NPs respectively (Table 4.2.2, entries 1 and 2). In case of Pd_{OS} NPs, significant amount of homocoupling product of aryl boronic acid was observed. We next opt to study the *in situ* catalytic effect of the aqueous plant extracts on the reaction progress. On using Ext AV, we were able to isolate 50% of the desired product using 1 mol% $Pd(OAc)_2$ in $EtOH/H_2O(1:1)$ as the reaction medium (Table 4.2.2, entry 3). On increasing the amount of Ext AV, a gradual increase in reaction yield was observed (Table 4.2.2, entries 4 and 5). Enhanced catalytic activity

was observed using 2 mL of Ext AV (Table 4.2.2, entry 5). However, on performing the reaction using Ext OS, relatively lower yield of cross-coupling product was obtained (Table 4.2.2, entries 6 and 7).

Table 4.2.2: Optimization of reaction conditions for Suzuki-Miyaura reaction [a]

$$R-\underset{}{\bigcirc}-Br + (HO)_2B-\bigcirc \xrightarrow[K_2CO_3, EtOH/H_2O, rt]{Pd(OAc)_2/Ext\ OS\ (or)\ Ext\ AV} R-\bigcirc-\bigcirc \quad R: OMe, NO_2$$

Entry	R	Pd Catalyst (mol%)	(Ext.) (mL)	Solvent (mL)	Base (mmol)	Time	Yield (%) [b]
1	4-NO$_2$	Pd$_{AV}$NP$_{ex\ situ}$(1)	-	EtOH/H$_2$O (1:1)	K$_2$CO$_3$	6h	30
2	4-NO$_2$	Pd$_{OS}$NP$_{ex\ situ}$(1)	-	EtOH/H$_2$O (1:1)	K$_2$CO$_3$	6h	10
3	4-NO$_2$	Pd(OAc)$_2$ (1)	Ext AV(0.5)	EtOH/H$_2$O (1:1)	K$_2$CO$_3$	1h	50
4	4-NO$_2$	Pd(OAc)$_2$ (1)	Ext AV (1)	EtOH/H$_2$O (1:1)	K$_2$CO$_3$	15min	70
5	4-NO$_2$	Pd(OAc)$_2$ (1)	Ext AV (2)	EtOH/H$_2$O (1:1)	K$_2$CO$_3$	15min	90
6	4-NO$_2$	Pd(OAc)$_2$ (1)	Ext OS (0.5)	EtOH/H$_2$O (1:1)	K$_2$CO$_3$	1h	40
7	4-NO$_2$	Pd(OAc)$_2$ (1)	Ext OS (2)	EtOH/H$_2$O (1:1)	K$_2$CO$_3$	1h	40
8	4-NO$_2$	Pd(OAc)$_2$ (1)	-	EtOH/H$_2$O (1:1)	K$_2$CO$_3$	1h	50
9	4-NO$_2$	Pd(OAc)$_2$ (0.5)	Ext AV (2)	EtOH/H$_2$O (1:1)	K$_2$CO$_3$	15min	40
10	4-NO$_2$	Pd(OAc)$_2$ (1)	Ext AV (2)	H$_2$O	K$_2$CO$_3$	15min	60
11	4-OMe	Pd(OAc)$_2$ (1)	Ext AV (2)	EtOH/H$_2$O (1:1)	K$_2$CO$_3$	15min	95
12	4-OMe	Pd(OAc)$_2$ (0.5)	Ext AV (2)	H$_2$O	K$_2$CO$_3$	15min	92
13	4-OMe	Pd(OAc)$_2$ (0.5)	Ext AV (2)	H$_2$O	NaOH	15min	78
14	4-OMe	Pd(OAc)$_2$ (0.5)	Ext AV (2)	H$_2$O	Na$_2$CO$_3$	15min	80
15	4-OMe	Pd(OAc)$_2$ (0.5)	Ext AV (2)	H$_2$O	Na$_2$PO$_4$	15min	85

[a] Reaction conditions: Aryl bromide (1 mmol), phenylboronic acid (1.2 mmol), solvent (2 mL) [b] Isolated yields

Since the phytochemical constituents in both the plant extract (Ext OS and Ext AV) varies in nature and composition (Table 4.2.1) [38-44], the catalytic efficiency in the coupling reaction seems to differ. Interestingly during the synthesis of Pd NPs using both
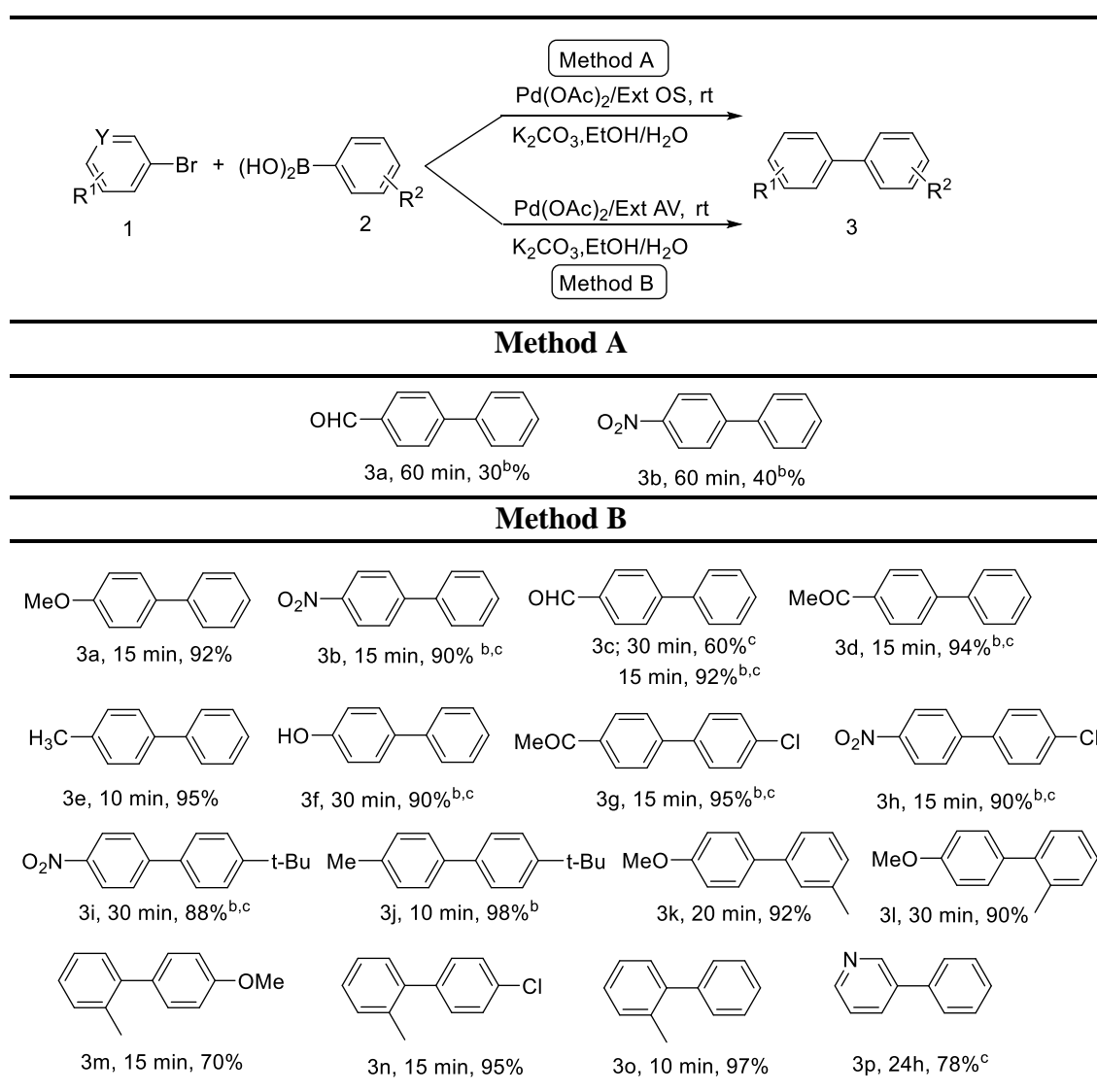
the plant extracts, we have observed that Ext OS was more effective than Ext AV and Pd$_{OS}$ NPs$_{ex\ situ}$ is formed quickly compared to Pd$_{AV}$ NPs$_{ex\ situ}$ (Figure 4.2.1). On the contrary, during the *in situ* experiments Ext OS was found to be less effective compared to Ext AV in Suzuki-Miyaura reaction. The cause of poorer conversion in case of Ext OS might be due to presence of aryl boronic acid. Liu et al in 2008 described the role of aryl boronic acid in the formation of NPs [56]. They had performed controlled experiment for *in situ* generation of NPs, and established that aryl boronic acid act as an associate reducing agent in the formation of NPs. Similar case was observed in the present protocol in the generation of *in situ* Pd$_{AV}$ NPs. As we have seen that in the synthesis of Pd$_{AV}$ NPs$_{ex\ situ}$ it requires longer time for the conversion of Pd(II) to Pd(0) nano without any chemical reducing agent. However, in the *in situ* catalytic approach, after addition of aryl boronic acid the Pd(II) ions immediately changes to black colour indicating the quickened formation of Pd NPs. UV/Vis spectra have also revealed the difference in reduction of Pd(II) ion. Moreover, aryl boronic acids act as a stabilizer for NPs and serve as a capping agent to keep them constant in size. This may sometimes lead to limitation of catalytic activity of NPs [57], which was observed in case of Pd$_{OS}$ NPs$_{in\ situ}$. Since the *Ocimum sanctum e*xtract (Ext OS) act a great reducing stabilizer in generation of NPs, the additional stabilizing effect of aryl boronic acid capped most of the free surface active site for catalysis resulting in weaker catalytic activity of the Pd$_{OS}$ NP$_{in\ situ}$. As such according to adsorption theory, activation of 4-bromonitrobenzene was diminished due to adsorption/capping of aryl boronic acid particulates in the catalyst surface resulting in poor reaction yield. Again, it is seen that in absence of either of the extracts, the reaction does not proceed efficiently, which reveal the significance of the plant extract in the reaction medium (Table 4.2.2, entry 8). Considering the higher activity of Pd$_{AV}$ NPs$_{in\ situ}$ in this Suzuki-Miyaura coupling, further optimization was done using Ext AV. The catalytic activity of the Pd$_{AV}$ NPs$_{in\ situ}$ was examined by lowering the amount of Pd(OAc)$_2$. But, significant decrease in reaction yield was observed (Table 4.2.2, entry 9). The catalytic efficiency was checked using water as the reaction medium. However, no appreciable result was obtained (Table 4.2.2, entry 10). This may be due to insolubility of the reactant species in water resulting in weaker coordination with the catalyst. Next, we have performed the reaction considering 4-bromoanisole and phenylboronic acid as the coupling partners. In this case the reaction seems to proceed efficiently in water as the reaction medium along with lower catalyst loading (Table 4.2.2, entries 11 & 12).

This is evidence of the solubility and coordination issue of the reactant species with the reaction medium and the catalyst. Then effect of different bases like NaOH, Na_2CO_3, and Na_2PO_4 have been studied, but superior catalytic activity was achieved only with K_2CO_3 (Table 4.2.2, entries 13-15 *vs* 12).

4.2.3.2.2. Substrate scope for Suzuki-Miyaura reaction

The catalytic system was studied for electronically diverse aryl bromides and aryl boronic acid. The reaction efficiency for both the methods using Ext OS and Ext AV was shown in Table 4.2.3.

Table 4.2.3: Substrate scope for Suzuki-Miyaura cross-coupling reaction [a]

Method A

3a, 60 min, 30[b]%

3b, 60 min, 40[b]%

Method B

3a, 15 min, 92%

3b, 15 min, 90% [b,c]

3c; 30 min, 60%[c]
15 min, 92%[b,c]

3d, 15 min, 94%[b,c]

3e, 10 min, 95%

3f, 30 min, 90%[b,c]

3g, 15 min, 95%[b,c]

3h, 15 min, 90%[b,c]

3i, 30 min, 88%[b,c]

3j, 10 min, 98%[b]

3k, 20 min, 92%

3l, 30 min, 90%

3m, 15 min, 70%

3n, 15 min, 95%

3o, 10 min, 97%

3p, 24h, 78%[c]

[a] Reaction conditions: Aryl bromides (0.5 mmol), aryl boronic acid (0.6 mmol), $Pd(OAc)_2$ (0.5 mol%), Ext (2 mL), H_2O (2 mL). [b] EtOH/H_2O (2 mL, 1:1), [c] 1 mol% $Pd(OAc)_2$

As already discussed, Method A (with Ext OS) did not shows diverse substrate compatibility. Method B (Ext AV) delivers excellent yield of cross-coupling product with electron donating substituent with lower catalyst loading in pure water as solvent (Table 4.2.3, 3a, 3e, 3k-o). Aryl halide bearing hydroxyl group on the other hand demands greater catalyst loading with EtOH as co-solvent (Table 4.2.3, 3f). The reaction was also compatible for electron withdrawing substituents affording excellent conversion in biphasic medium. However, slightly greater amount of catalyst was required in comparison to electron donating aryl bromides (Table 4.2.3, 3b-d, 3g-i). It is observed that electronically varied aryl boronic acid does not affect the reaction yield. However, *t*-butylphenylboronic acid requires biphasic condition for effective coupling. This may be due to solubility issue of the substrate in water (Table 4.2.3, 3j). The effectiveness of Method B was examined for heteroaryl halide, moderate yield of the cross-coupling product was achieved although greater reaction time was required (Table 4.2.3, 3p).

4.2.3.2.3. Recyclability of Pd$_{AV}$ NPs$_{in\ situ}$ in Suzuki-Miyaura reaction

Since, the recyclability of the catalyst is one of the most important factors in a reaction protocol. We next investigated the recyclability of the catalytic species using 4-bromoanisole (2 mmol) and phenylboronic acid (2.4 mmol) as the coupling partners. After the first catalytic cycle, the reaction mixture was extracted with ethyl acetate followed by centrifugation. The clearly separated organic fraction was removed and evaporated to get the crude product. The residue catalyst was washed with EtOH and then directly reused for the next catalytic run with the addition of fresh reactants, base and solvent.
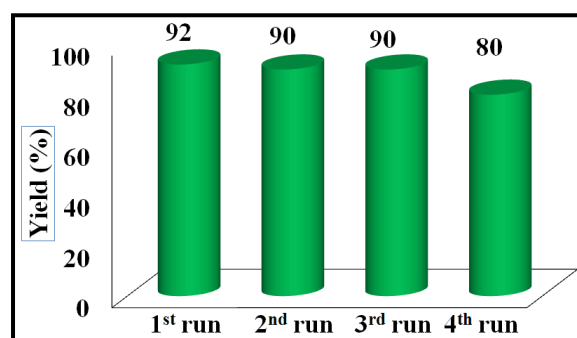

Figure 4.2.7: Reusability of Pd$_{AV}$ NPs$_{in\ situ}$ in Suzuki-Miyaura cross-coupling reaction

The reaction affords similar reactivity till 3rd cycle (Figure 4.2.7). However slight decrease in catalytic activity was observed in the 4th cycle with slight longer reaction

time. After the 2nd catalytic cycle, the morphology of the Pd$_{AV}$ NPs$_{in\ situ}$ was studied by TEM and HRTEM analysis. The TEM images show spherical NPs of Pd/PdO for Pd$_{AV}$ NPs$_{in\ situ}$ (Figure 4.2.8 a, b and c). Most of the Pd/PdO NPs were agglomerated during the reaction course. Therefore, the size of the NPs after the 2nd catalytic cycle is not clearly determinable. However, the lattice fringes are visible in the HRTEM image (Figure 4.2.8 d). The lattice fringe distance was found to be 0.22 nm corresponds to Pd (111) crystallographic plane.
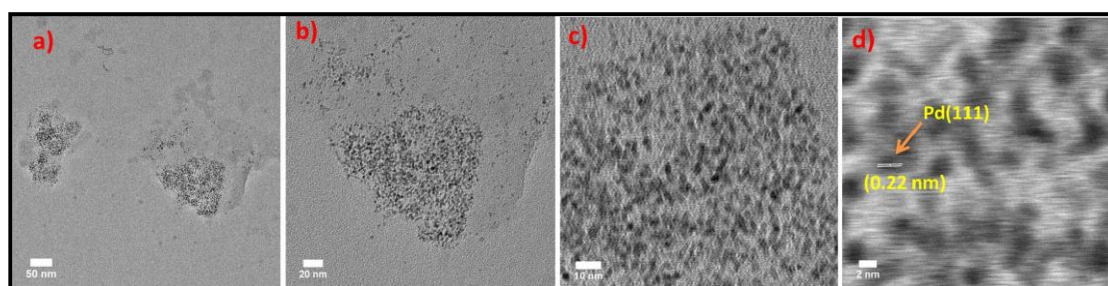
Figure 4.2.8: TEM (**a**,**b** and **c**) and high-resolution TEM (HRTEM) images (**d**) of Pd$_{AV}$ NPs$_{in\ situ}$ after 2nd catalytic cycle

Further, the catalytic activity of the *ex situ* and *in situ* generated Pd NPs were examined in Sonogashira cross-coupling of aryl halides and terminal alkynes.

4.2.3.2.4. Optimization of reaction conditions for Sonogashira reaction

Initially, we have performed the reaction using 4-iodonitrobenzene (0.5 mmol) and phenylacetylene (0.6 mmol) as our screening substrate in EtOH and K$_2$CO$_3$ as base at 40°C. The results are summarized in Table 4.2.4. The catalytic activity of both the *ex situ* generated Pd NPs were examined. We have noticed a significant difference in reactivity in comparison to the Suzuki-Miyaura cross-coupling reaction. Superior catalytic activity was observed using Pd$_{OS}$ NPs with 95% of cross-coupling product (Table 4.2.4, entry 1). A comparatively lower conversion was observed for Pd$_{AV}$ NPs with extended reaction time (Table 4.2.4, entry 2). Similar observation was achieved in case of *in situ* approach with Ext OS (Pd$_{OS}$ NP$_{in\ situ}$) being more competent than Ext AV (Pd$_{AV}$ NP$_{in\ situ}$) (Table 4.2.4, entries 3 & 4). Pd$_{OS}$ NP$_{in\ situ}$ affords greater yield within shorter reaction time, which may be due to the greater reducing and stabilizing effect of the extract in the reaction medium (Table 4.2.4, entries 1 *vs* 3). Considering the enhanced catalytic activity of Pd$_{OS}$ NP$_{in\ situ}$, further screening of the reaction was performed using these conditions. At room temperature, the reaction delivers lower yield of cross-coupled product (Table

4.2.4, entry 5). On increasing the amount of Ext OS, the yield of product slightly decreases (Table 4.2.4, entry 6). The difference in reaction yield on varying the amount of extract (Table 4.2.4 entries 3 vs 6) may be due to greater capping of free Pd surface sites by the plant extract, which as a result lowers the accessibility of the Pd NPs particle at the surface for catalysis [58,59].

Table 4.2.4: Optimization of reaction conditions for Sonogashira reaction [a]

Entry	Catalyst (mol%)	Extract (mL)	Solvent (mL)	Base (mmol)	Time (h)	Yield (%) [b]
1	$Pd_{os}NP_{ex\ situ}$(1)	-	EtOH	K_2CO_3	3	95
2	$Pd_{AV}NP_{ex\ situ}$(1)	-	EtOH	K_2CO_3	10	78
3	$Pd(OAc)_2$ (1)	Ext OS (0.5)	EtOH	K_2CO_3	2	97
4	$Pd(OAc)_2$ (1)	Ext AV (2)	EtOH	K_2CO_3	8	88
5	$Pd(OAc)_2$ (1)	Ext OS (0.5)	EtOH	K_2CO_3	3	82[c]
6	$Pd(OAc)_2$ (1)	Ext OS (1)	EtOH	K_2CO_3	2	95
7	$Pd(OAc)_2$ (1)	-	EtOH	K_2CO_3	4	60
8	$Pd(OAc)_2$ (0.5)	Ext OS (0.5)	EtOH	K_2CO_3	6	50
9	$Pd(OAc)_2$ (1)	Ext OS (0.5)	EtOH	Cs_2CO_3	2	97[d]
10	$Pd(OAc)_2$ (1)	Ext OS (0.5)	EtOH	Na_2CO_3	6	60
11	$Pd(OAc)_2$ (1)	Ext OS (0.5)	EtOH	$NaHCO_3$	6	20
12	$Pd(OAc)_2$ (1)	Ext OS (0.5)	EtOH	NaOAc	12	70
13	$Pd(OAc)_2$ (1)	Ext OS (0.5)	EtOH	NaOH	3	80
14	$Pd(OAc)_2$ (1)	Ext OS (0.5)	H_2O	K_2CO_3	24	40
15	$Pd(OAc)_2$ (1)	Ext OS (0.5)	$EtOH/H_2O$	K_2CO_3	12	40
16	$Pd(OAc)_2$ (1)	Ext OS (0.5)	2-MeTHF	K_2CO_3	24	nr
17	$Pd(OAc)_2$ (1)	Ext OS (0.5)	2-MeTHF/ H_2O (1:1)	K_2CO_3	24	20
18	$Pd(OAc)_2$ (1)	Ext OS (0.5)	THF	K_2CO_3	12	30
19	$PdCl_2$(1)	Ext OS (0.5)	EtOH	K_2CO_3	4	85
20	$Pd(OAc)_2$ (1)	Ext OS (0.5)	EtOH	K_2CO_3	3	85 [e]

[a] Reaction conditions: 4-iodonitrobenzene (0.5mmol), phenylacetylene (0.6 mmol), base (1.5 mmol), solvent (4mL) at 40°C [b] Isolated yield [c] rt [d] Cs_2CO_3(1 mmol) [e] 4-iodonitrobenzene (0.5 mmol), phenylacetylene (0.5 mmol)

Moreover, in absence of Ext OS the reaction bears very minimum conversion, which signifies their role and importance for the present cross-coupling reaction (Table 4.2.4, entry 7). On lowering the amount of $Pd(OAc)_2$, the reaction efficiency decreases (Table 4.2.4, entry 8). Next we have screened the Sonogashira cross-coupling for different bases. Activity of various inorganic bases such as Cs_2CO_3, Na_2CO_3, $NaHCO_3$, $NaOAc$ and $NaOH$ were studied (Table 4.2.4, entries 9-13). However, greater efficiency was achieved only in case of K_2CO_3 and Cs_2CO_3 (Table 4.2.4, entries 3 & 9). But considering the cost and hygroscopic nature of Cs_2CO_3, we opt for the readily available and low cost K_2CO_3 for our reaction protocol. Again the efficiency of the catalyst was checked using different solvent system. Use of pure water or biphasic medium such as $EtOH$-H_2O (1:1) significantly decreases the yield of the product (Table 4.2.4, entries 14 and 15). Other solvents such as 2-MeTHF, 2-MeTHF/H_2O (1:1) and THF do not meet to our expectation in terms of isolated yield (Table 4.2.4, entries 16-18). Later, considering the optimized reaction condition, the coupling reaction was also tested for different palladium source such as $PdCl_2$. But, lower conversion of desired product was noticed (Table 4.2.4, entry 19). This lower activity of $PdCl_2$ in the present reaction system may be due to difference in coordination of anion ($Cl^- < OAc^-$) to the nanoparticle surface. Thus lower efficacy of Cl^- anion towards stabilization of nanostructure may hamper the catalytic performance [17,60] we have carried out our reaction using 1:1 ratio of the substrates (Table 4.2.4, entry 20). But, a significant decrease in reaction efficiency was observed.

4.2.3.2.5. Substrate scope for Sonogashira reaction

Electronically different substrates were examined to verify the catalytic activity of Method A and Method B for Sonogashira coupling (Table 4.2.5). Method B, as already discussed provides lower efficiency in terms of yield and time (Table 4.2.5, 6a, b & c). Method A provides efficient cross-coupling for diverse range of substrates (Table 4.2.5, 6d-6u). It is compatible for aliphatic alkynes which in general is low reactive in nature (Table 4.2.5, 6q-6u) [5,61]. Aryl iodides bearing electron withdrawing groups in *p-* and *m-* position proceed to completion of reaction with excellent yield of cross-coupling product (Table 4.2.5, 6d, 6f, 6g, 6l-p). However, electron donating aryl iodides are less competent in comparison to the later (Table 4.2.5, 6h & 6i). The variation in reaction efficiency may be due to electronic effect of the substituents. Since presence of electron donating group increases the electron density over sp^2 carbon and halide bond which as a

result causes difficulty in C-X bond breaking for oxidative addition step [62]. Again, steric effect as in case of 2-iodonitrobenzene results low yield of product (Table 4.2.5, 6j).

Table 4.2.5: Substrate scope for Sonogashira cross-coupling reaction [a]

Method B

6a: R^1 = 4-NO$_2$, R^2 = C$_6$H$_5$, X= I, 88%, 8h

6b: R^1 = 4-OCH$_3$, R^2 = C$_6$H$_5$, 70%, 8h

6c: R^1 = 4-CH$_3$, R^2 = C$_6$H$_5$, X = I, 80%, 6h

Method A

6d: R^1= 4-NO$_2$, R^2 = C$_6$H$_5$, X= I, 97%, 2h, X = Br, 50%^{c}, 80^0 C, 24h

6e: R^1 = H, R^2 = C$_6$H$_5$, X = I, 90%, 4h, X = Br, 70%, 4h

6f: R^1 = 3-NO$_2$, R^2 = C$_6$H$_5$, 98%, 3.5h

6g: R^1 = 4-COMe, R^2 = C$_6$H$_5$, 97%, 3.5h

6h: R^1 = 4-CH$_3$, R^2 = C$_6$H$_5$, X = I, 85%, 3h, X = Br, 80^0 C, 65%, 24h

6i: R^1 = 4-OCH$_3$, R^2 = C$_6$H$_5$, 70%, 4h

6j: R^1 =2-NO$_2$, R^2 = C$_6$H$_5$, X = I, 30%, 12h

6k: R^1 = H, R^2 = 4-CH$_3$, X = I, 85%, 4h

6l: R^1 = H, R^2 = 4-CH$_3$, X = I, 90%, 2.5h

6m: R^1 = 4-COMe, R^2 = C$_6$H$_5$, 95%, 3.5h

6n: R^1 = 4-NO$_2$, R^2 = 4-OCH$_3$, 88%, 4h

6o: R^1 = 4-COMe, R^2 = 3-CH$_3$, 92%, 6h

6p: R^1 = 3-CHO, R^2 = 3-CH$_3$, X= I, 95%, 6h

6q: R^1 = H, R^2= C$_4$H$_9$, X= I, 85%, 8h

6r: R^1 = H, R^2= octyl, X= I, 75%, 10h

6s: R^1 = 4H, R^2= Cyclohexyl, X= I, 80%, 10h

6t: R^1 = 4-CH$_3$, R^2= C$_4$H$_9$, X= I, 80%, 10h

6u: R^1 = 4-NO$_2$, R^2= C$_4$H$_9$, X= I, 40%, 10h

[a] Reaction conditions: aryl halide (0.5 mmol), acetylene (0.6 mmol), Pd(OAc)$_2$ (1mol %), Ext OS (0.5 mL), Ext AV (2 mL), K$_2$CO$_3$ (1.5 mmol), EtOH (4 mL).[b] Isolated yield

The effect of different aromatic and aliphatic alkynes was investigated. The catalytic system delivers similar conversion in case of different substituted aromatic alkynes (Table 4.2.5, 6k-6p). Slightly longer reaction time is required for aliphatic alkynes, nevertheless in all cases modest to good yield of desired product was achieved (Table 4.2.5, 6q-6u). However a difference in reactivity of 1-hexyne was observed with 4-iodonitrobenzene and 4-iodotoluene (Table 4.2.5, 6t & 6u). Iodobenzene in all cases offers comparable catalytic performance in terms of both reaction yield and time (Table 4.2.5, 6e, 6k & 6q-6s). Next, we have tried to extend our catalytic system for aryl bromides. Since C-Br activation is difficult in comparison to C-I, coupling of substituted aryl bromides was found to be difficult. Only 50-65% of isolated yield was achieved for p-NO$_2$ and p-CH$_3$ substituent of aryl bromide respectively (Table 4.2.5, 6d & 6h). Bromobenzene on the other hand delivers good yield of desired cross coupled product within shorter reaction time (Table 4.2.5, 6e). However the reaction did not proceed with aryl chlorides.

4.2.3.3. Hot filtration test

To identify the catalysis nature of both the Pd NPs (Pd$_{AV}$ NPs$_{in\ situ}$, and Pd$_{OS}$ NPs$_{in\ situ}$), in the reaction medium, we have performed the hot filtration test considering both the cross-coupling reaction using the optimized reaction conditions. To do this, the reactions were performed considering the model substrates and optimized reaction conditions. The reaction was monitored *via* TLC and after 50% conversion (1.5h); the reaction mixture was filtered. After filtration, the filtrate reaction mixture was allowed to stir for additional 1.5h. The reaction was monitored vide TLC and no further increase in product formation was observed. This proves the heterogeneous nature of the catalytic system. Hence, both the *in situ* generated Pd NPs are heterogeneous in nature.

However, as per the recyclability of the Pd$_{OS}$ NPs$_{in\ situ}$ in Sonogashira coupling reaction, the catalyst could not be recovered after the workup. This may be due to smaller particle sizes which might gets solubilized in the water or ethylacetate. However, in Suzuki-Miyaura coupling, boronic acid stabilized and capped the Pd NPs and as such prevents the Pd NPs to dissociates into smaller aggregates.

4.2.4. Conclusions

In summary, the present catalytic system highlights the different reducing potential of two naturally abundant herbs found over worldwide and focuses on one pot biogenic generation of Pd NPs under aerobic condition without use of any additional chemical

reducing agent. The process appears as an excellent alternative for many ligand assisted system for C-C coupling. Moreover, significant influence of the substrates on the catalytic activity of the biogenic Pd NPs has been observed in Sonogashira and Suzuki-Miyaura cross coupling reactions.

4.2.5. Analytical data of the synthesized biaryl derivatives
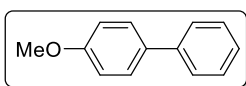
4-Methoxybiphenyl: (Table 4.2.3, 3a): White Solid, m.p. 81-83 °C, **^{1}H NMR (400 MHz, CDCl$_3$):** 7.56-7.51 (m, 4H), 7.41-7.39 (m, 2H), 7.31-7.24 (m, 1H), 6.97 (d, 2H, J = 8.7 Hz), 3.84 (s, 3H) ppm. **^{13}C NMR (100 MHz, CDCl$_3$):** δ 159.2, 140.9, 133.8, 128.8, 128.2, 126.8, 126.7, 114.2, 55.4 ppm.
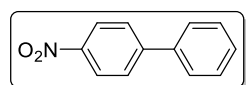
4-Nitrobiphenyl: (Table 4.2.3, 3b): Yellow Solid, m.p. 113-115 °C, **^{1}H NMR (400 MHz, CDCl$_3$):** δ 8.29 (d, 2H, J = 8.7 Hz), 7.73 (d, 2H, J = 8.7 Hz), 7.63-7.61 (m, 2H), 7.51-7.44 (m, 3H) ppm. **^{13}C NMR (100 MHz, CDCl$_3$):** δ 147.7, 138.8, 129.2, 128.9, 127.8, 127.4, 124.1, 120.0, ppm.
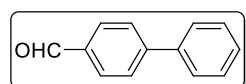
4-Formylbiphenyl: (Table 4.2.3, 3c): White Solid, m.p. 57-59 °C, **^{1}H NMR (400 MHz, CDCl$_3$):** δ 10.05 (s, 1H), 7.95 (d, 2H, J = 8.2 Hz), 7.75 (d, 2H, J = 8.2 Hz), 7.64-7.62 (m, 2H), 7.49-7.39 (m, 3H) ppm. **^{13}C NMR (100 MHz, CDCl$_3$):** δ 192.0, 147.3, 139.8, 135.2, 130.3, 129.1, 128.5, 127.7, 127.4 ppm.
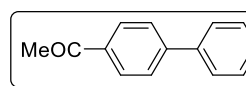
4-Acetylbiphenyl: (Table 4.2.3, 3d): White Solid, m.p. 118-120 °C, **^{1}H NMR (400 MHz, CDCl$_3$):** 8.03 (d, 2H, J = 8.0 Hz), 7.68 (d, 2H, J = 8.0 Hz), 7.62 (d, 2H, J = 7.3 Hz), 7.49-7.39 (m, 3H), 2.64 (s, 3H) ppm. **^{13}C NMR (100 MHz, CDCl$_3$):** δ 197.8, 145.8, 139.9, 135.9, 129.0, 128.9, 128.3, 127.3, 26.7 ppm.
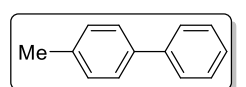
4-Methylbiphenyl: (Table 4.2.3, 3e): White Solid, m.p. 46-48 °C, **^{1}H NMR (400 MHz, CDCl$_3$):** 7.57 (d, 2H, J = 7.7 Hz), 7.49 (d, 2H, J = 7.7 Hz), 7.43-7.39 (m, 2H), 7.33-7.31 (m, 1H) 7.25-7.23 (m, 2H), 2.39 (s, 3H) ppm. **^{13}C NMR (100 MHz, CDCl$_3$):** δ 141.3, 138.5, 137.2, 129.7, 128.9, 127.4, 127.3, 127.2, 21.3 ppm.
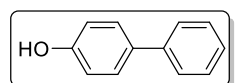
4-Hydroxybiphenyl: (Table 4.2.3, 3f): Light brown Solid, m.p. 164-168 °C, **^{1}H NMR (400 MHz, CDCl$_3$):** 7.54-7.24 (m, 7H), 6.90 (d, 1H, J = 8.2 Hz), 6.72-6.69 (m, 1H), 5.07 (s, 1H) ppm. **^{13}C NMR (100 MHz, CDCl$_3$):** δ 155.1, 140.8, 132.5, 128.8, 128.4, 126.8, 117.3, 115.7 ppm.
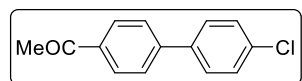
4-Acetyl-4′-chlorobiphenyl: (Table 4.2.3, 3g): White Solid,

m.p. 104-106 °C, **^{1}H NMR (400 MHz, CDCl$_3$):** δ 8.02 (d, 2H, *J* = 8.2 Hz), 7.64 (d, 2H, *J* = 8.7 Hz), 7.55 (d, 2H, *J* = 8.7 Hz), 7.43 (d, 2H, *J* = 8.7 Hz), 2.63 (s, 3H) ppm. **^{13}C NMR (100 MHz, CDCl$_3$):** δ 197.7, 144.5, 138.3, 136.1, 134.5, 129.3, 129.0, 128.5, 127.1, 26.7 ppm.
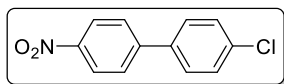
4-Chloro-4′-nitrobiphenyl: (Table 4.2.3, 3h): Pale Yellow Solid, m.p. 142-145 °C, **^{1}H NMR (400 MHz, CDCl$_3$):** δ 8.30 (d, 2H, *J* = 8.7 Hz), 7.71 (d, 2H, *J* = 8.7 Hz), 7.54 (d, 2H, *J* = 8.7 Hz), 7.47 (d, 2H, *J* = 8.7 Hz) ppm. **^{13}C NMR (100 MHz, CDCl$_3$):** δ 146.4, 137.2, 135.3, 129.4, 129.0, 128.7, 127.7, 124.3 ppm.
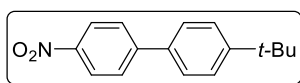
4-Nitro-4′-t-butylbiphenyl: (Table 4.2.3, 3i): Pale yellow Solid, m.p. 110-112 °C, **^{1}H NMR (400 MHz, CDCl$_3$):** 8.27 (d, 2H, *J* = 8.7 Hz), 7.72 (d, 2H, *J* = 8.7 Hz), 7.58-7.49 (m, 4H), 1.36 (s, 9H) ppm. **^{13}C NMR (100 MHz, CDCl$_3$):** δ 152.3, 147.5, 135.8, 132.5, 127.6, 127.1, 126.2, 124.2, 34.8, 31.3 ppm.
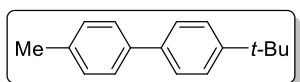
4-Methyl-4′-t-butylbiphenyl: (Table 4.2.3, 3j): White Solid, m.p. 120-124 °C, **^{1}H NMR (400 MHz, CDCl$_3$):** 7.53-7.44 (m, 6H), 7.25-7.22 (m, 2H), 2.38 (s, 3H), 1.36 (s, 9H) ppm. **^{13}C NMR (100 MHz, CDCl$_3$):** δ 150.0, 138.3, 136.7, 129.4, 127.0, 126.9, 126.6, 125.7, 55.4, 34.5, 21.1 ppm.
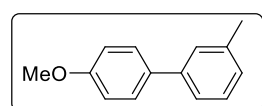
4-Methoxy-3′-methylbiphenyl: (Table 4.2.3, 3k): White Solid, m.p. 48-49 °C, **^{1}H NMR (400 MHz, CDCl$_3$):** 7.53-7.50 (m, 2H), 7.36-7.24 (m, 3H), 7.12 (d, 1H, *J* = 7.3 Hz), 6.98-6.95 (m, 2H), 3.85 (s, 3H), 2.40 (s, 3H) ppm. **^{13}C NMR (100 MHz, CDCl$_3$):** δ 159.1, 140.8, 138.3, 133.9, 128.7, 128.2, 127.6, 127.4, 123.9, 114.2, 55.4, 21.6 ppm.
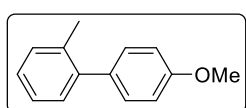
4-Methoxy-2′-methylbiphenyl: (Table 4.2.3, 3l): Colourless liquid, **^{1}H NMR (400 MHz, CDCl$_3$):** 7.26-7.21 (m, 6H), 6.96-6.82 (m, 2H), 3.85 (s, 3H), 2.27 (s, 3H) ppm. **^{13}C NMR (100 MHz, CDCl$_3$):** δ 158.5, 141.6, 135.5, 134.4, 130.4, 130.3, 129.9, 127.0, 125.8, 113.5, 55.3, 20.6 ppm.
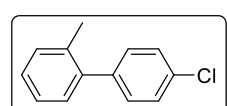
**4-Chloro-2′-methylbiphenyl: (Table 4.2.3, 3n):** Colourless liquid, **^{1}H NMR (400 MHz, CDCl$_3$):** 7.48-7.37 (m, 6H), 7.28-7.20 (m, 2H), 2.26 (s, 3H) ppm. **^{13}C NMR (100 MHz, CDCl$_3$):** δ 135.3, 133.8, 130.6, 130.5, 129.7, 129.1, 128.3, 127.6, 125.9, 20.4 ppm.
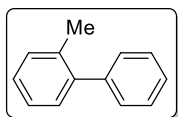
2-Methylbiphenyl: (Table 4.2.3, 3o): Colourless liquid, **¹H NMR (400 MHz, CDCl₃):** 7.68 (d, 1H, *J* = 7.7 Hz), 7.54-7.48 (m, 3H), 7.42-7.41 (m, 2H), 7.35-7.33 (m, 3H), 2.37 (s, 3H) ppm. **¹³C NMR (100 MHz, CDCl₃):** δ 135.5, 132.5, 130.5, 129.9, 129.3, 128.9, 128.2, 127.4, 127.3, 126.9, 125.9, 20.6 ppm.
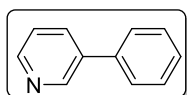
3-Phenylpyridine: (Table 4.2.3, 3p) Colourless liquid, **¹H NMR (400 MHz, CDCl₃):** δ 8.68 (s, 1H), 8.53-8.51 (m, 3H), 7.86-7.83 (m, 2H), 7.24-7.18 (m, 3H) ppm. **¹³C NMR (100 MHz, CDCl₃):** δ 156.6, 150.6, 147.4, 139.3, 129.6, 125.1, 121.2, 120.1, 115.5 ppm.
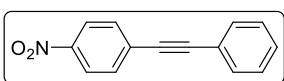
1-Nitro-4-(2-phenylethynyl)benzene (Table 4.2.5, 6d): Yellow Solid, m.p. 119-121 °C, **¹H NMR (400 MHz, CDCl₃):** δ 8.22 (d, *J* = 9.0 Hz, 2H), 7.68-7.66 (m, 2H), 7.57-7.55 (m, 2H), 7.40-7.26 (m, 3H).ppm. **¹³C NMR (100 MHz, CDCl₃):** δ 147.0, 132.3, 131.9, 130.3, 129.3, 128.6, 123.7, 122.1, 94.8, 87.2 ppm.
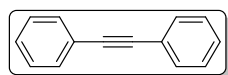
Diphenylacetylene (Table 4.2.5, 6e): White Solid, m.p. 54-56 °C, **¹H NMR (400 MHz, CDCl₃):** δ 7.54-7.52 (m, 4H), 7.34-7.22 (m, 6H) ppm. **¹³C NMR (100 MHz, CDCl₃):** δ 131.7, 128.4, 128.3, 123.3, 89.4 ppm.
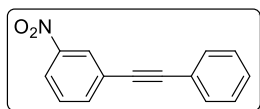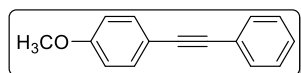
1-Nitro-3-(2-phenylethynyl)benzene (Table 4.2.5, 6f): Yellow gum, **¹H NMR (400 MHz, CDCl₃):** δ 8.35 (s, 1H), 8.17 (d, 1H, *J* = 8.2 Hz), 7.81 (d, 1H, *J* = 7.3 Hz), 7.56-7.50 (m, 3H), 7.37-7.24 (m, 3H) ppm. **¹³C NMR (100 MHz, CDCl₃):** δ 148.2, 137.3, 131.9, 129.4, 129.2, 128.6, 126.5, 125.2, 122.9, 122.3, 92.0, 86.9 ppm.
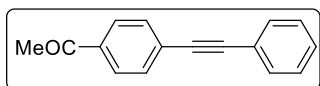
1-Acetyl-4-(2-phenylethynyl)benzene (Table 4.2.5, 6g): White Solid, m.p. 94-96 °C, **¹H NMR (400 MHz, CDCl₃):** δ 7.97-7.88 (m, 2H), 7.65-7.58 (m, 2H), 7.57-7.50 (m, 2H), 7.39-7.32 (m, 3H), 2.60 (s, 3H).ppm. **¹³C NMR (100 MHz, CDCl₃):** δ 197.4, 136.2, 131.8, 128.9, 128.5, 128.3, 128.2, 122.7, 92.7, 88.6, 26.7 ppm.
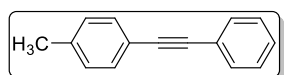
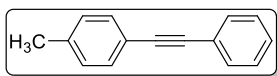**1-Methyl-4-(2-phenylethynyl)benzene (Table 4.2.5, 6h):** White solid, m.p. 68-70 °C, **¹H NMR (400 MHz, CDCl₃):** δ 7.53-7.50 (m, 2H), 7.42 (d, 2H, *J* = 8.2 Hz), 7.33-7.23 (m, 3H), 7.14 (d, 2H, *J* = 8.2 Hz), 2.35 (s, 3H) ppm. **¹³C NMR (100 MHz, CDCl₃):** δ 138.4, 132.5, 131.6, 129.3, 129.2, 128.1, 123.5, 120.2, 89.6, 88.7, 21.6 ppm.
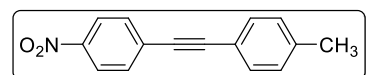
1-Methoxy-4-(2-phenylethynyl)benzene (**Table 4.2.5, entry**

6i): White solid, m.p. 79-81 °C, **^{1}H NMR (400 MHz, CDCl$_3$)**, δ 7.51-7.44 (m, 4H), 7.32-7.30 (m, 3H), 6.86 (d, J = 8.7 Hz, 2H), 3.82 (s, 3H) ppm. **^{13}C NMR (100 MHz, CDCl$_3$):** δ 159.7, 133.1, 131.5, 128.4, 128.0, 123.7, 115.4, 114.1, 89.9, 89.4, 55.4 ppm.
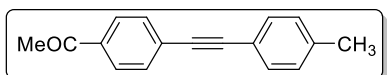

1-Methyl-4-(2-phenylethynyl)benzene (Table 4.2.5, entry 6k): White solid, m.p. 68-70 °C, **^{1}H NMR (400 MHz, CDCl$_3$):** δ 7.53-7.51 (m, 2H), 7.42 (d, 2H, J = 8.2 Hz), 7.35-7.32 (m, 3H), 7.15 (d, 2H, J = 8.2 Hz), 2.36 (s, 3H) ppm.**^{13}C NMR (100 MHz, CDCl$_3$):** δ 138.4, 137.3, 132.5, 131.6, 131.5, 129.3, 129.2, 128.5, 128.1, 123.5, 120.2, 89.6, 88.7, 21.6 ppm.
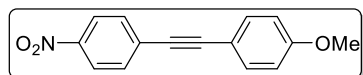

1-Methyl-4-[2-(4-nitrophenyl)ethynyl]benzene (Table 4.2.5, 6l): Light yellow solid, mp 149-151 °C, **^{1}H NMR (400 MHz, CDCl$_3$):** δ 8.20 (d, 2H, J = 8.2 Hz), 7.63 (d, 2H, J = 8.7 Hz), 7.44 (d, 2H, J = 7.7 Hz), 7.18 (d, 2H, J = 7.7 Hz), 2.38 (s, 3H) ppm. **^{13}C NMR (100 MHz, CDCl$_3$):** δ 146.9, 139.7, 132.2, 131.8, 130.6, 129.4, 123.7, 119.1, 95.1, 87.1, 21.7 ppm.
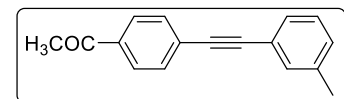

1-Acetyl-4-[2-(4-methylphenyl)ethynyl]benzene (Table 4.2.5, 6m): White solid, m.p. 125-127 °C, **^{1}H NMR (400 MHz, CDCl$_3$):** δ 7.92 (d, 2H, J = 8.2 Hz), 7.58 (d, 2H, J = 8.7 Hz), 7.43 (d, 2H, J = 8.2 Hz), 7.16 (d, 2H, J = 8.2 Hz), 2.60 (s, 3H), 2.37 (s, 3H) ppm. **^{13}C NMR (100 MHz, CDCl$_3$):** δ 197.4, 139.1, 136.1, 131.7, 129.4, 128.5, 128.3, 119.6, 93.1, 87.2, 26.7, 21.6 ppm.


1-Methoxy-4-[2-(4-nitrophenyl)ethynyl]benzene (Table 4.2.5, 6n): Light yellow solid, mp 111-112 °C, **^{1}H NMR (400 MHz, CDCl$_3$):** δ 8.19 (d, 2H, J = 9.16 Hz), 7.62 (d, 2H, J =9.16 Hz), 7.49 (d, 2H, J = 8.2 Hz), 6.91-6.88 (m, 2H), 3.83 (s, 3H) ppm.**^{13}C NMR (100 MHz, CDCl$_3$):** δ 160.4, 146.7, 133.5, 132.0, 130.8, 123.7, 114.3, 114.2, 95.2, 86.7, 55.4 ppm.

**1-Acetyl-4-[2-(3-methylphenyl)ethynyl]benzene (Table 4.2.5, 6o):** White solid, m.p. 110-114 °C, **^{1}H NMR (400 MHz, CDCl$_3$):** δ 7.93 (d, 2H, J = 8.2 Hz), 7.59 (d, 2H, J = 8.7 Hz), 7.44 (d, 2H, J = 8.2 Hz), 7.17 (d, 2H, J = 8.2 Hz), 2.61 (s, 3H), 2.38 (s, 3H) ppm. **^{13}C NMR (100 MHz, CDCl$_3$):** δ 197.4, 139.1, 136.1, 131.7, 131.6, 129.3, 128.5, 128.4, 128.3, 119.6, 93.1, 88.1, 26.6, 21.6 ppm.
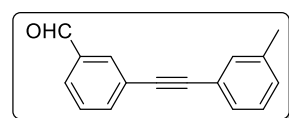

1-Formyl-3-[2-(3-methylphenyl)ethynyl]benzene (Table 4.2.5, 6p): Yellow gum, **^{1}H NMR (400 MHz, CDCl$_3$):** δ 10.01 (s, 1H), 8.27-8.01 (m, 4H), 7.85-7.16 (m, 4H) ppm. **^{13}C NMR**

(100 MHz, CDCl₃): δ 191.6, 170.3, 138.2, 129.7, 129.5, 129.1, 128.8, 128.6, 128.4, 128.3, 124.7, 124.1, 122.5, 99.9, 87.5, 21.2 ppm.
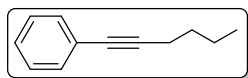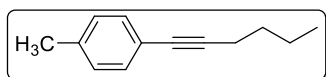
 1-(Hex-1-yn-1-yl)-benzene (Table 4.2.5, 6q): yellow liquid; **^{1}H NMR (400 MHz, CDCl₃):** δ 7.40-7.38 (m, 2H), 7.27-7.25 (m, 3H), 2.41 (*t*, 2H, *J* = 6.8 Hz), 1.60-1.45 (m, 4H), 0.94 (*t*, 3H, *J* = 7.3 Hz) ppm. **^{13}C NMR (100 MHz, CDCl₃)**: δ 131.6, 128.2, 127.5, 124.1, 90.5, 80.6, 29.7, 22.7, 19.1, 13.5 ppm.
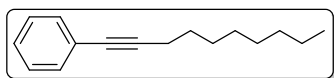
 1-(Dodec-1-yn-1-yl)-benzene (Table 4.2.5, 6r): yellow liquid; 1H NMR (400 MHz, CDCl₃): δ 7.40-7.37 (m, 2H), 7.27-7.25 (m, 3H), 2.39 (t, 2H, *J* = 6.8 Hz), 1.62-1.27 (m, 12H), 0.88 (t, 3H, *J* = 6.8 Hz) ppm. 13C NMR (100 MHz, CDCl₃): δ 131.6, 128.2, 127.5, 124.1, 90.5, 80.6, 32.0, 29.7, 29.4, 29.2, 28.8, 22.7, 19.4, 14.2 ppm.
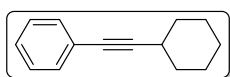
 1-(Cyclohexylethynyl)benzene (Table 4.2.5, 6s): Yellow liquid, **^{1}H NMR (400 MHz, CDCl₃):** δ 7.40-7.38 (m, 2H), 7.29-7.25 (m, 3H), 2.59-2.57 (m, 1H), 1.89-1.34 (m, 10H) ppm. **^{13}C NMR (100 MHz, CDCl₃):** δ 131.9, 131.6, 128.3, 128.2, 127.4, 94.5, 87.2, 35.1, 32.7, 26.0, 25.4, 24.9, 23.4, 22.8 ppm.

 1-(Hex-1-yn-1-yl)-4-methylbenzene (**Table 4.2.5, 6t**), Yellow liquid, **^{1}H NMR (400 MHz, CDCl₃):** δ 7.29-7.06 (m, 2H), 7.08-7.06 (m, 2H), 2.41-2.37 (m, 2H), 2.32 (s, 3H), 1.60-1.46 (m, 4H), 0.96-0.92 (m, 3H) ppm.**^{13}C NMR (100 MHz, CDCl₃):** δ 137.4, 131.4, 129.1, 128.0, 89.6, 80.6, 30.9, 22.1, 21.4, 19.2. 13.7 ppm.

^{1}H and ^{13}C NMR spectra of 4-Methoxy-2′-methylbiphenyl
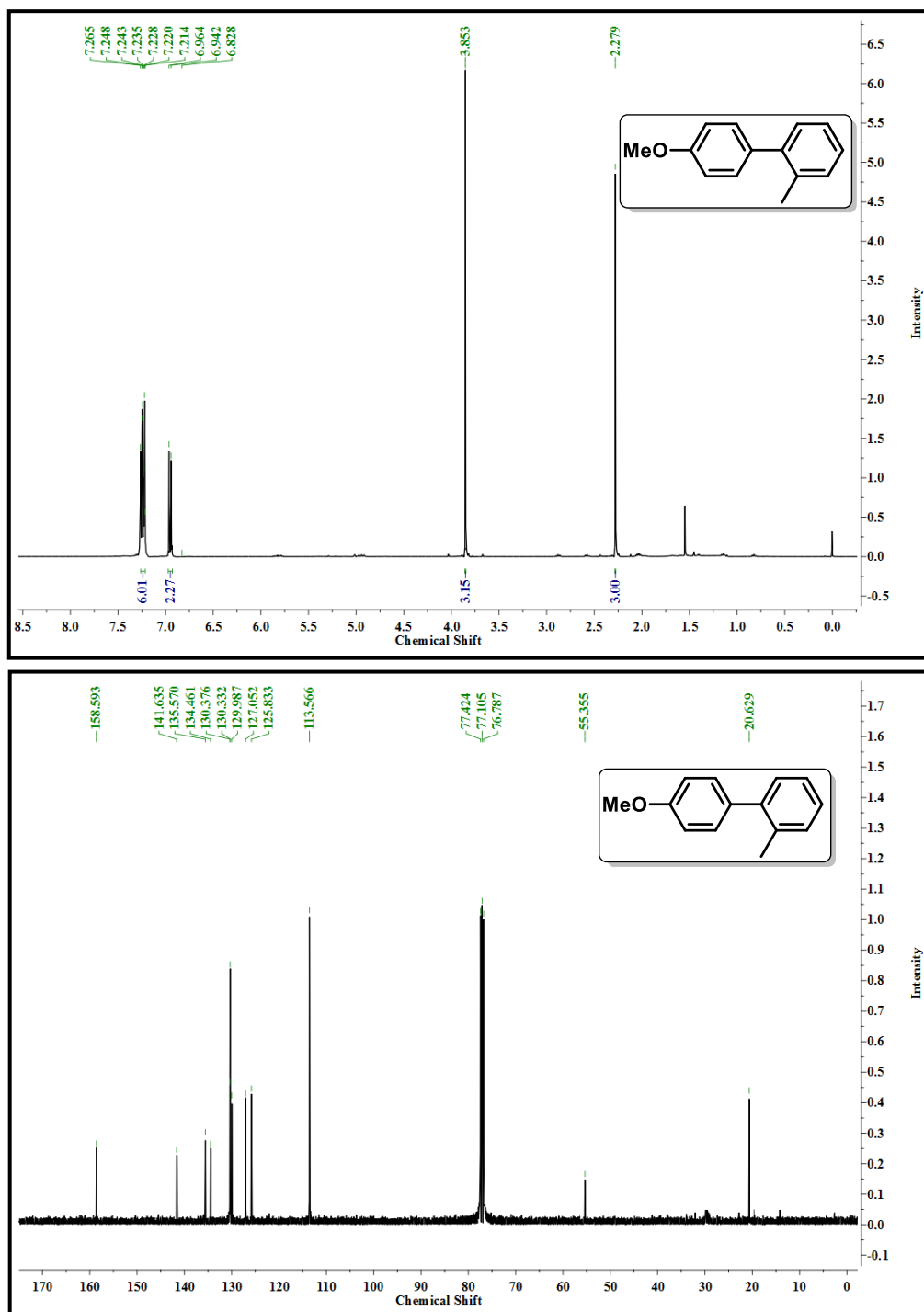
^{1}H and ^{13}C NMR spectra of 1-Nitro-3-(2-phenylethynyl)
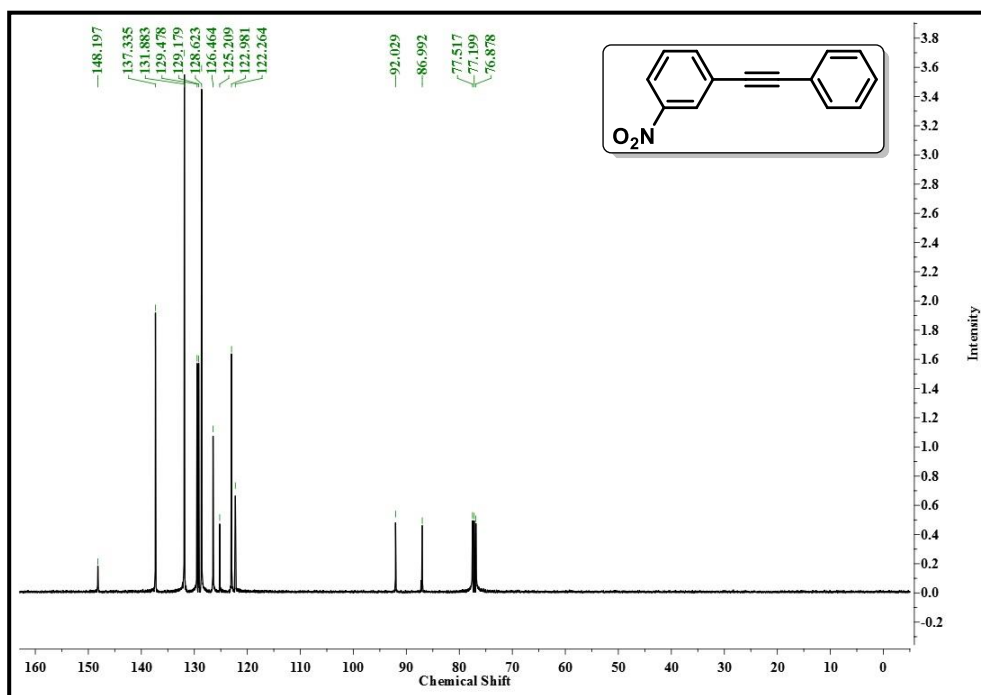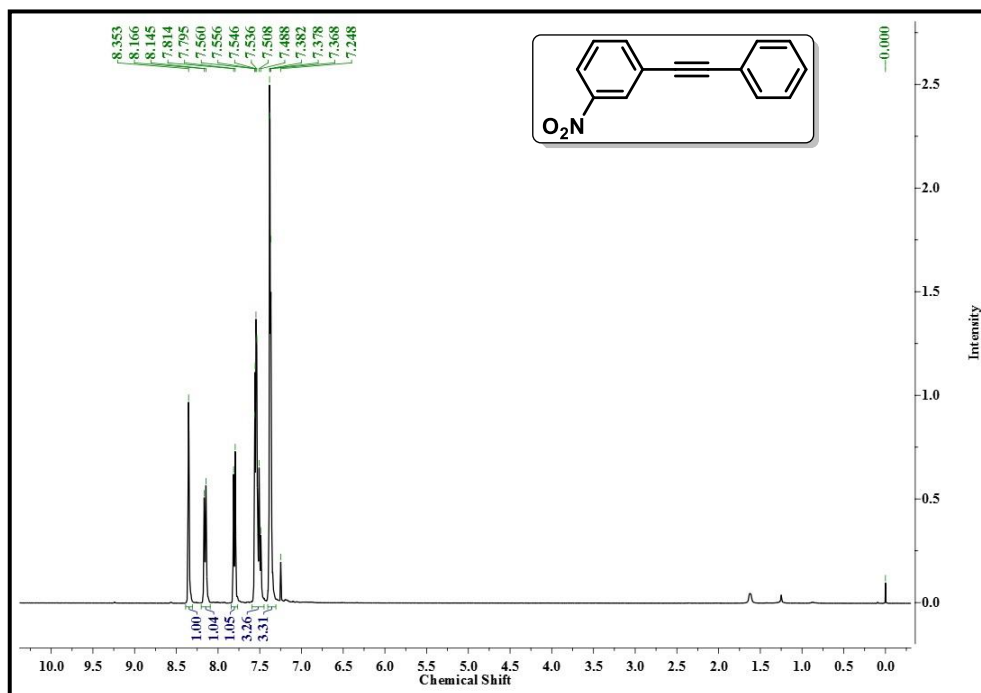
4.3. References

[1] Cosford, N. D., Tehrani, L., Roppe, J., Schweiger, E., Smith, N. D., Anderson, J., Bristow, L., Brodkin, J., Jiang, X., McDonald, I., Rao, S., Washburn, M., and Varney, M. A., 3-[(2-Methyl-1,3-thiazol-4-yl)ethynyl]-pyridine: A potent and highly selective metabotropic glutamate subtype 5 receptor antagonist with anxiolytic activity. *Journal of Medicinal Chemistry*, 46(2):204-206, 2003.

[2] Bagley, M. C., Dale, J. W., Merritt, E. A., and Xiong, X. Thiopeptide antibiotics. *Chemical Reviews*, 105(2):685-714, 2005.

[3] Tykwinski, R. R. Evolution in the palladium-catalyzed cross-coupling of sp- and sp^2-hybridized carbon atoms. *Angewandte Chemie International Edition*, 42(14):1566-1568, 2003.

[4] Sonogashira, K. Development of Pd–Cu catalyzed cross-coupling of terminal acetylenes with sp^2-carbon halides. *Journal of Organometallic Chemistry*, 653(1-2):46-49, 2002.

[5] Chinchilla, R. and Nájera, C. Recent advances in Sonogashira reactions. *Chemical Society Reviews*, 40(10):5084-5121, 2011.

[6] Nishihara, Y., Ikegashira, K., Hirabayashi, K., Ando, J. I., Mori, A., and Hiyama, T. Coupling reactions of alkynylsilanes mediated by a Cu(I) Salt: Novel syntheses of conjugate diynes and disubstituted ethynes. *The Journal of Organic Chemistry*, 65(6):1780-1787, 2000.

[7] Glaser, C. Untersuchungen Über Einige Derivate der Zimmtsäure. *Justus Liebigs Annalen der Chemie*, 154(2):137-171, 1870.

[8] Hay, A. S. Oxidative coupling of acetylenes. *The Journal of Organic Chemistry*, 27(9):3320-3321, 1962.

[9] Elangovan, A., Wang, Y. H., and Ho, T. I. Sonogashira coupling reaction with diminished homocoupling. *Organic Letters*, 5(11):1841-1844, 2003.

[10] Nyberg, C. and Tengstål, C. G. Adsorption and reaction of water, oxygen, and hydrogen on Pd(100): Identification of adsorbed hydroxyl and implications for the catalytic H_2–O_2 reaction. *The Journal of Chemical Physics*, 80(7):3463-3468, 1984.

[11] Scoccia, J., Perretti, M. D., Monzón, D. M., Crisóstomo, F. P., Martín, V. S., and Carrillo, R. Sustainable oxidations with air mediated by gallic acid: potential applicability in the reutilization of grape pomace. *Green Chemistry*, 18(9):2647-2650, 2016.

[12] Balanta, A., Godard, C., and Claver, C. Pd nanoparticles for C–C coupling reactions. *Chemical Society Reviews*, 40(10):4973-4985, 2011.

[13] González-Centeno, M. R., Jourdes, M., Femenia, A., Simal, S., Rosselló, C., and Teissedre, P. L. Characterization of polyphenols and antioxidant potential of white grape pomace byproducts (Vitis Vinifera L.). *Journal of Agricultural and Food Chemistry*, 61(47):11579-11587, 2013.

[14] Kambourakis, S., Draths, K. M., and Frost, J. W. Synthesis of gallic acid and pyrogallol from glucose: Replacing natural product isolation with microbial catalysis. *Journal of the American Chemical Society*, 122(37):9042-9043, 2000.

[15] Narayanan, R. and El-Sayed, M. A. Effect of catalysis on the stability of metallic nanoparticles: Suzuki reaction catalyzed by PVP-palladium nanoparticles. *Journal of the American Chemical Society*, 125(27):8340-8347, 2003.

[16] Durand, J., Teuma, E., and Gomez, M. An overview of palladium nanocatalysts: surface and molecular reactivity. *European Journal of Inorganic Chemistry*, 2008(23):3577-3586, 2008.

[17] Finke, R. G. and Özkar, S. Molecular insights for how preferred oxoanions bind to and stabilize transition-metal nanoclusters: A tridentate, C3 symmetry, lattice size-matching binding model. *Coordination Chemistry Reviews*, 248(1-2):135-146, 2004.

[18] Ko, Y. L., Krishnamurthy, S., and Yun, Y. S. Facile synthesis of monodisperse Pt and Pd nanoparticles using antioxidants. *Journal of Nanoscience and Nanotechnology*, 15(1):412-417, 2015.

[19] Mondal, M., Begum, T., Gogoi, P. K., and Bora, U. Gallic acid derived palladium(0) nanoparticles: an *insitu* formed "green and recyclable" catalyst for Suzuki-Miyaura coupling in water. *ChemistrySelect*, 1(15):4645-4651, 2016.

[20] Ghoreishi, S. M., Behpour, M., Khayatkashani, M., and Motaghedifard, M. H. simultaneous determination of ellagic and gallic acid in punica granatum, myrtus communis and itriphal formulation by an electrochemical sensor based on a carbon paste electrode modified with multi-walled carbon nanotubes. *Analytical Methods*, 3(3):636-645, 2011.

[21] Lee, J., Koh, K., and Hwang, S. Density functional theoretical study on the reduction potentials of catechols in water. *Bulletin of the Korean Chemical Society*, 33(11):3889-3890, 2012.

[22] Yu, K., Sommer, W., Weck, M., and Jones, C. W. Silica and polymer-tethered pd–scs-pincer complexes: evidence for precatalyst decomposition to form soluble catalytic species in Mizoroki–Heck chemistry. *Journal of Catalysis*, 226(1):101-110, 2004.

[23] Phan, N. T., Van Der Sluys, M., and Jones, C. W. On the nature of the active species in palladium catalyzed Mizoroki–Heck and Suzuki–Miyaura couplings–homogeneous or heterogeneous catalysis, A critical review. *Advanced Synthesis & Catalysis*, 348(6):609-679, 2006.

[24] Badhani, B., Sharma, N., and Kakkar, R. Gallic ccid: A versatile antioxidant with promising therapeutic and industrial applications. *RSC Advances*, 5(35):27540-27557, 2015.

[25] Jain, K. K. Applications of nanobiotechnology in clinical diagnostics. *Clinical Chemistry*, 53(11):2002-2009, 2007.

[26] Jackson, T. C., Patani, B. O., and Ekpa, D. E. Nanotechnology in diagnosis: A review. *Advances in Nanoparticles*, 6(03):93-102, 2017.

[27] Mody, V. V., Siwale, R., Singh, A., and Mody, H. R. Introduction to metallic nanoparticles. *Journal of Pharmacy and Bioallied Sciences*, 2(4):282-289, 2010.

[28] Biffis, A., Centomo, P., Del Zotto, A., and Zecca, M. Pd metal catalysts for cross-couplings and related reactions in the 21st century: A critical review. *Chemical Reviews*, 118(4):2249-2295, 2018.

[29] Das, V. K., Borah, M., and Thakur, A. J. Piper-betle-shaped nano-s-catalyzed synthesis of 1-amidoalkyl-2-naphthols under solvent-free reaction condition: A greener "Nanoparticle-Catalyzed Organic Synthesis Enhancement" approach. *The Journal of Organic Chemistry*, 78(7):3361-3366, 2013.

[30] Das, V. K., Harsh, S. N., and Karak, N. Highly efficient and active silver nanoparticle catalyzed conversion of aldehydes into nitriles: a greener, convenient, and versatile 'NOSE' approach. *Tetrahedron Letters*, 57(5):549-553, 2016.

[31] Ghorbani, H. R., Safekordi, A. A., Attar, H., and Sorkhabadi, S. M. Biological and non-biological methods for silver nanoparticles synthesis. *Chemical and Biochemical Engineering Quarterly*, 25(3):317-326, 2011.

[32] Duan, H., Wang, D., and Li, Y. Green chemistry for nanoparticle synthesis. *Chemical Society Reviews*, 44(16):5778-5792, 2015.

[33] Ingale, A. G. and Chaudhari, A. N. Biogenic synthesis of nanoparticles and potential applications: An eco-friendly approach. *Journal of Nanomedicine and Nanotechology*, 4(165):1-7, 2013.

[34] Vishnukumar, P., Vivekanandhan, S., and Muthuramkumar, S. Plant-mediated biogenic synthesis of palladium nanoparticles: recent trends and emerging opportunities. *ChemBioEng Reviews*, 4(1):18-36, 2017.

[35] Mittal, A. K., Chisti, Y., and Banerjee, U. C. Synthesis of metallic nanoparticles using plant extracts. *Biotechnology Advances*, 31(2):346-356, 2013.

[36] Biajoli, A. F., Schwalm, C. S., Limberger, J., Claudino, T. S., and Monteiro, A. L. Recent progress in the use of Pd-catalyzed C-C cross-coupling reactions in the synthesis of pharmaceutical compounds. *Journal of the Brazilian Chemical Society*, 25(12):2186-2214, 2014.

[37] Gogoi, N., Bordoloi, P., Borah, G., and Gogoi, P. K. Synthesis of palladium nanoparticle by bio-reduction method and its effectiveness as heterogeneous catalyst towards selective oxidation of benzyl alcohols in aqueous media. *Catalysis Letters*, 147(2):539-546, 2017.

[38] Vidhani, S. I., Vyas, V. G., Parmar, H. J., Bhalani, V. M., Hassan, M. M., Gaber, A., and Golakiya, B. A. Evaluation of some chemical composition, minerals fatty acid profiles, antioxidant and antimicrobial activities of tulsi (Ocimum Sanctum) from India. *American Journal of Food Science and Technology*, 4:52-7, 2016.

[39] Kashif, M. and Ullah, S. Chemical composition and minerals analysis of hippophae rhamnoides, azadirachta indica, punica granatu and ocimum sanctum leaves. *World Journal of Dairy & Food Sciences*, 8(1):67-73, 2013.

[40] Bhargawa, S., Kapoor, S., Ranote, P. S., and Sharma, S. Studies on aloe juice supplemented Kinnow Nectar. *Research Journal of Agriculture and Forestry Sciences*, 2(8):14-20, 2014.

[41] Hamid, G. H., El-Kholany, E. A., and Nahla, E. A. Evaluation of aloe vera gel as antioxidant and antimicrobial ingredients in orange-carrot blend nectars. *Middle East Journal of Agriculture Research*, 3(4):1122-1134, 2014.

[42] Zhang, A., Liu, M., Liu, M., Xiao, Y., Li, Z., Chen, Z., Sun, Y., Zhao, J., Fang, S., Jia, D., and Li, F. Homogeneous Pd nanoparticles produced in direct reactions: green synthesis, formation mechanism and catalysis properties. *Journal of Materials Chemistry A*, 2(5):1369-1374, 2014.

[43] Camp, J. E., Dunsford, J. J., Cannons, E. P., Restorick, W. J., Gadzhieva, A., Fay, M. W., and Smith, R. J. Glucose-derived palladium(0) nanoparticles as in situ-formed catalysts for Suzuki–Miyaura cross-coupling reactions in isopropanol. *ACS Sustainable Chemistry & Engineering*, 2(3):500-505, 2014.

[44] Dewan, A., Bharali, P., Bora, U., and Thakur, A. J. Starch assisted palladium(0) nanoparticles as *in situ* generated catalysts for room temperature Suzuki–Miyaura reactions in water. *RSC Advances*, 6(14):11758-11762, 2016.

[45] Chil Núñez, I., Escalona Arranz, J C., Berenguer Rivas, C A., Mendonça, P M., Mateo Pérez K., Dutok Sánchez, C M., Cortinhas, L B., Silva, C F., Carvalho, M G., Queiroz, M M C. Chemical composition and toxicity of Ocimum sanctum l. var. cubensis essential oil up-growing in the eastern of cuba, *International Journal of Pharmacognosy and Phytochemical Research*, 9(7):1021-1028, 2017.

[46] Hussain, A. I., Chatha, S. A. S., Kamal, G. M., Ali, M. A., Hanif, M. A., and Lazhari, M. I. Chemical composition and biological activities of essential oil and extracts from Ocimum Sanctum. *International Journal of Food Properties*, 20(7):1569-1581, 2017.

[47] Saroj, T. and Krishna, A. A Comparison of Chemical Composition and Yield of Essential Oils from Shoot System parts of Ocimum sanctum found in semi-arid region of Uttar Pradesh, *Agrotechnology*, 6(3):172, 2017.

[48] Ahmed, M. and Hussain, F. Chemical Composition and biochemical activity of *Aloe Vera* (*Aloe Barbadensis* Miller) leaves. *International Journal of Chemical and Biochemical Sciences*, 3:29-33, 2013.

[49] Boudreau, M. D. and Beland, F. A. An evaluation of the biological and toxicological properties of Aloe Barbadensis (Miller), Aloe Vera. *Journal of Environmental Science and Health Part C*, 24(1):103-154, 2006.

[50] Ahlawat, K. S. and Khatkar, B. S. Processing, food applications and safety of aloe vera products: A review. *Journal of Food Science and Technology*, 48(5):525-533, 2011.

[51] Šoptrajanova, L. and Šoptrajanov, B. Vibrational studies of palladium(II) acetate compounds I. infrared spectra of hexa-μ-acetato-triangulo-tripalladium-water (2/1). *Spectroscopy Letters*, 25(7):1131-1139, 1992.

[52] Banse, B. A. and Koel, B. E. Interaction of oxygen with Pd(111): High effective O_2 pressure conditions by using nitrogen dioxide. *Surface Science*, 232(3):275-285, 1990.

[53] Bindhani, B. K. and Panigrahi, A. K. Biosynthesis and characterization of silver nanoparticles (SNPs) by using leaf extracts of Ocimum Sanctum L (Tulsi) and study of its antibacterial activities. *Journal of Nanomedicine & Nanotechnology*, (S6):1-5, 2015.

[54] Rao, Y. S., Kotakadi, V. S., Prasad, T. N. V. K. V., Reddy, A. V., and Gopal, D. S. Green synthesis and spectral characterization of silver nanoparticles from lakshmi tulasi (Ocimum Sanctum) leaf extract. *Spectrochimica Acta Part A: Molecular and Biomolecular Spectroscopy*, 103:156-159, 2013.

[55] Harraz, F. A., El-Hout, S. E., Killa, H. M., and Ibrahim, I. A. Palladium nanoparticles stabilized by polyethylene glycol: efficient, recyclable catalyst for hydrogenation of styrene and nitrobenzene. *Journal of Catalysis*, 286:184-192, 2012.

[56] Han, W., Liu, C., and Jin, Z. Aerobic ligand-free Suzuki coupling reaction of aryl chlorides catalyzed by in situ generated palladium nanoparticles at room temperature. *Advanced Synthesis & Catalysis*, 350(3):501-508, 2008.

[57] Sarmah, M., Mondal, M., Gohain, S. B., and Bora, U. Gallic acid-derived palladium(0) nanoparticles as in situ-formed catalyst for Sonogashira cross-coupling reaction in ethanol under open air. *Catalysis Communications*, 90:31-34, 2017.

[58] Liu, W. and Wang, H. Influence of surface capping on oxygen reduction catalysis: A case study of 1.7 nm Pt nanoparticles. *Surface Science*, 648:120-125, 2016.

[59] Ahmed, S., Ahmad, M., Swami, B. L., and Ikram, S. Green synthesis of silver nanoparticles using azadirachta indica aqueous leaf extract. *Journal of Radiation Research and Applied Sciences*, 9(1):1-7, 2016.

[60] Thathagar, M. B., Kooyman, P. J., Boerleider, R., Jansen, E., Elsevier, C. J., and Rothenberg, G. Palladium nanoclusters in Sonogashira cross-coupling: A true catalytic species?. *Advanced Synthesis & Catalysis*, 347(15):1965-1968, 2005.

[61] Liu, C., Bao, F., and Ni, Q. Palladium-Catalyzed Phosphine-, Copper-free and aerobic Sonogashira coupling in aqueous media. *ARKIVOC*, 11:60-68, 2011.

[62] Schilz, M. and Plenio, H. A guide to Sonogashira cross-coupling reactions: The influence of substituents in aryl bromides, acetylenes, and phosphines. *The Journal of Organic Chemistry*, 77(6):2798-2807, 2012.